LUND UNIVERSITY

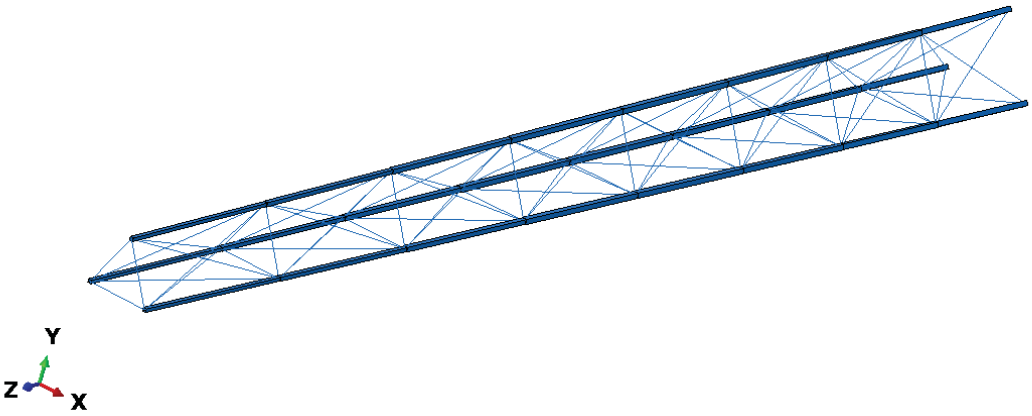

DESIGN OF WIND TURBINE BLADES WITH RESPECT TO STABILITY

OSKAR LINDKVIST and VICTOR NICOLAUSSON

Structural Mechanics

Master's Dissertation

DEPARTMENT OF CONSTRUCTION SCIENCES

DIVISION OF STRUCTURAL MECHANICS

ISRN LUTVDG/TVSM--19/5241--SE (1-67) | ISSN 0281-6679

MASTER'S DISSERTATION

DESIGN OF WIND TURBINE BLADES WITH RESPECT TO STABILITY

OSKAR LINDKVIST and VICTOR NICOLAUSSON

Supervisor: Professor **KENT PERSSON**, Division of Structural Mechanics, LTH.

Examiner: Professor **PER-ERIK AUSTRELL**, Division of Structural Mechanics, LTH.

Printed by V-husets tryckeri LTH, Lund, Sweden, January 2020 *(Pl)*.

For information, address:
Division of Structural Mechanics,
Faculty of Engineering LTH, Lund University, Box 118, SE-221 00 Lund, Sweden.
Homepage: www.byggmek.lth.se

Contents

List of Figures

List of Tables

Dimensionering av vindkraftverksblad med hänsyn till stabilitet

Oskar Lindkvist & Victor Nicolausson

Sammanfattning

Under 2000-talet har vindkraftverk tagit plats som en av de främsta lösningarna i samhällets strävan efter en koldioxidfri energiproduktion. Vindkraften har vuxit parallellt med framsteg inom andra områden, och utveckling inom t.ex. materialteknik har möjliggjort längre blad och en större energiproduktion. I grunden är dock den övergripande designen på vindkraftverk relativt oförändrad.

Winfoor är i processen att utveckla ett nytt rotorblad, Triblade, med målet att bryta den trenden. Triblade använder tre individuella blad orienterade i en fackverkskonstruktion. Tack vare fackverkskonstruktionen kan strukturen assembleras från flera mindre delar, vilket drar ner på kostnaderna och underlättar vid både tillverkning och transport. Därtill är designen lättare än konventionella blad av samma längd, och öppnar därmed upp för materialval, som t.ex. stål.

Målet med arbetet är att studera möjligheterna kring att använda stål i strutkturen, till skillnad från konventionella material så som kol- och glasfiberkompositer. Detta med fokus på strukturens stabilitet på både lokal och global nivå.

Studierna som visas i arbetet har utvärderat; materialvalet stål, användning av korrugerade balktvärsnitt samt olika infästningsmöjligheter. Påverkan hos kraftspelet av globala parametrar så som infästningsmetod, bladseparation och bladvinkling har också utretts. Utvärderingarna är utförda med finita element metoden (FEM) där både linjära och olinjära analyser har utförts.

De linjära analyserna har som syfte att beräkna bucklingsmoderna av strukturen för den obelastade konstruktionen. Dessa moder används sedan som initiella geometriska imperfektioner till den olinjära analysen, som tar hänsyn till stora deformationer.

De två mäktigaste slutsatserna i arbetet är att materialvalet stål är ett fullgot alternativ i denna konstruktion samt att korrugerade balktvärsnitt ökar mängden last som strukturen kan utsättas för innan buckling sker, och att materialmängden därmed kan minskas.

Design of wind turbine blades with respect to stability

Oskar Lindkvist & Victor Nicolausson

Abstract

In the 21st century, wind power has emerged as a strong candidate in fulfilling societies goals of achieving carbon-free energy energy production. Windpower has evolved along with other technological developments, giving rise to larger turbines, but with the overall design trend remaining largely unchanged.

Winfoor, a Swedish company based in Lund, aims to break that trend. With their new Triblade design, Winfoor hopes to change the way wind turbine blades. Here, the traditional single airfoil is replaced by three smaller foils, utilizing a truss system to retain structural integrity. The truss-design also allows for a modular assembly, as opposed to the traditional design which is constructed as a single piece. This allows for a simpler production(construction), transport and erection process. The design also has the potential to be significantly lighter than it's conventional counterparts.

This thesis studies the possibility of using steel as opposed to more conventional materials such as carbon and glass fibre reinforced polymers. Specifically, the stability of the structure with respect to global and local buckling is examined during hurricane-force winds, when the wind turbine is not producing electricity.

The possibility of improving structural stability using corrugated beams is studied using finite element software, where a combination of linear and non-linear procedures is used. The impact of changes to the overall design, such as connection methods and distance between the blades, is also studied.

The analysis consists of two parts; a linear buckling analysis of the structure, followed by a general static analysis of the structure under load, where the calculated buckling modes are applied as initial imperfections in order to capture any post-buckling behaviour.

From this thesis it was concluded that corrugated beams significantly improve the stability of the structure while also allowing for the use of steel, as opposed to more expensive conventional materials.

Acknowledgements

This master's dissertation concludes our five years at Lund University and our master's degree in Structural- and Civil engineering. The thesis was carried out for Winfoor and the paper was published by The Division of Structural Mechanics at Lund University Faculty of Engineering.

We would like to thank Professor Kent Person for supervising our work and supporting us whenever help was needed. Thanks are also due to PhD-students Karin Forsman and Jens Malmborg for their assistance in Abaqus and Python. We would also like to thank Rikard Berthilsson, Pascal Rubin and all of their colleagues at Winfoor AB for their help and knowledge.

Thanks also go out to the staff at Lunarc, without which the large number of simulations would not have been possible.

As this thesis marks the end of our engineering studies in Lund we would like to thank our mothers, fathers, brothers, sisters and friends for all your love and support over these years.

Lund, June 2019
Oskar Lindkvist, Victor Nicolausson

1 Introduction

1.1 Background

The 21st century has seen the rise of wind power as a viable and integral part in fulfilling society's goal of achieving carbon free energy production. This brings with it a demand for improved technology in order to increase efficiency and decrease costs. The length of turbine blades has continued to increase, but the fundamental design has remained relatively unchanged.

With their new Triblade design, Winfoor aims to break that trend. Triblade uses three individual blades instead of one, oriented in a triangular pattern, with a truss system providing structural integrity. By utilizing a truss system, it is possible to split the entire wing structure into several smaller segments. The purpose of this is to make the structure lighter and cheaper than it's competitors, while also making it easier to manufacture and transport.

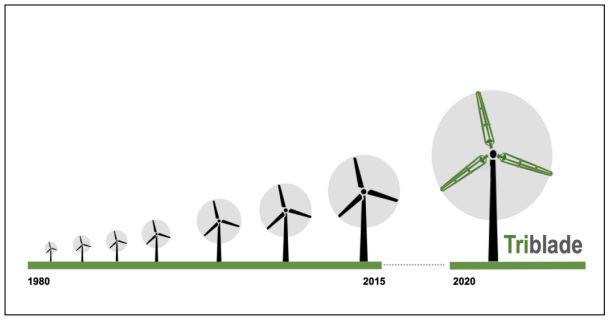

Figure 1.1: The historic development of wind turbine blades and the ambitions for the Triblade.(*Drag Coefficient*)

Most turbines are designed using fibre reinforced polymers, mainly fiberglass (GFRP) and carbon (CFRP) fiber. Both materials are advantageous in that they are resistant to fatigue, have a low density and a high stiffness. They also share a disadvantage, namely that they are expensive when compared to more conventional materials such as steel. As with any product, cost is a critical factor. It would therefore be advantageous if steel could be used instead of GFRP's and CFRP's. Due to limitations on weight, the load-carrying beams in such a structure would need to be as thin as possible. This, in combination with the high compressive forces involved in certain load cases, puts much emphasis on the stability of the beams.

1.2 Objective and method

The objective of this thesis is to determine one or more beam types, constructed using steel, that fulfill Winfoor's goals with respect to weight and structural integrity during the stand still load case, discussed further in chapter 4.5. *ABAQUS CAE*, a software designed for calculations using the finite element method, was used to examine which cross section that best could meet these demands. The general process is described below.

- Develop a parametric model in Abaqus using Python. The Python script is written such that it is easy to implement a wide range of cross sections, definable by the user.
- For a given cross sectional type, determine buckling modes and critical load of the global structure.
- Apply the calculated modes as initial imperfections in a static general analysis, with regard to large deformations and plastic material properties.
- If the entire load can be applied in the static general step, the cross section is deemed sufficient. The cross section is then subjected to the same load but with a smaller thickness. This process is reiterated until only one or a few cross sections remain, where the ones remaining are considered stable. These are then evaluated with regards to stress, deformation and global parameters.

Due to cross sections with different shapes having different stiffness, and thereby impacting the buckling mode eigenvalues of the structure, it was determined that it was necessary to be able to implement arbitrary cross sections in the global model.

The ambitions considering the weight of the structure is that it should not weigh more than a normal turbine blade, wich is about 25 tonnes för a 90 m rotorblade.

1.3 Limitations

In this thesis, a number of limitations and simplifications have been introduced.

- The production load case was not considered in this thesis. This is mainly due to that, in general, the stand still load case is the most unfavorable one when considering stability.
- The hub connection will not be considered. It will be assumed to have an infinite stiffness resulting in that the Triblade will be acting like a cantileaver beam
- Dynamic response was not considered.
- The impact of the geometry on aerodynamical properties was neglected as the focus of this thesis is to optimize the structural mechanics of the blade.

- The model is restricted to cross sectional types that can be defined by a set of vertices. Cross sections defined by continuous curves, e.g. circular sections, are not possible.

1.4 Outline of thesis

Chapter 1:	**Introduction**
	Describes the background-, aim and limitations of the thesis
Chapter 2:	**Wind turbine blade design**
	In this chapter tratitional wind tubine blade design and the triblade technology are discussed.
Chapter 3:	**Theory**
	In this chapter the basic theory of the finite element method, element types and buckling are discussed.
Chapter 4:	**Finite element model**
	In this chapter the modelling techniques used to establish the FE-model are discussed.
Chapter 5:	**Results**
	In this chapter the results from the Finite element analyzes conducted on the different configurations are discussed.
Chapter 6:	**Conclusion**
	In this chapter the conclusions made from the thesis are discussed
	Bibliography
	Reference list of literature used

2 Wind turbine blade design

In this section the triblade design including; geometry, material and the loading of the blade is described.

2.1 Traditional wind turbine blade design

Most wind turbines in use today are designed as traditional horizontal-axis wind turbines (HAWT), indicating that they use three individual blades, usually built in one piece using composite materials, such as, glass and carbon fibre. When designing turbine blades one must consider both aerodynamic and structural aspects.

The aerodynamics of the blade will impact it's efficiency when producing energy, while the structural aspects will determine it's ability to withstand the loads expected during it's lifetime. A brief introduction to the aerodynamic properties of airfoils will be given, along with a description of the unique structural design of the Triblade system.

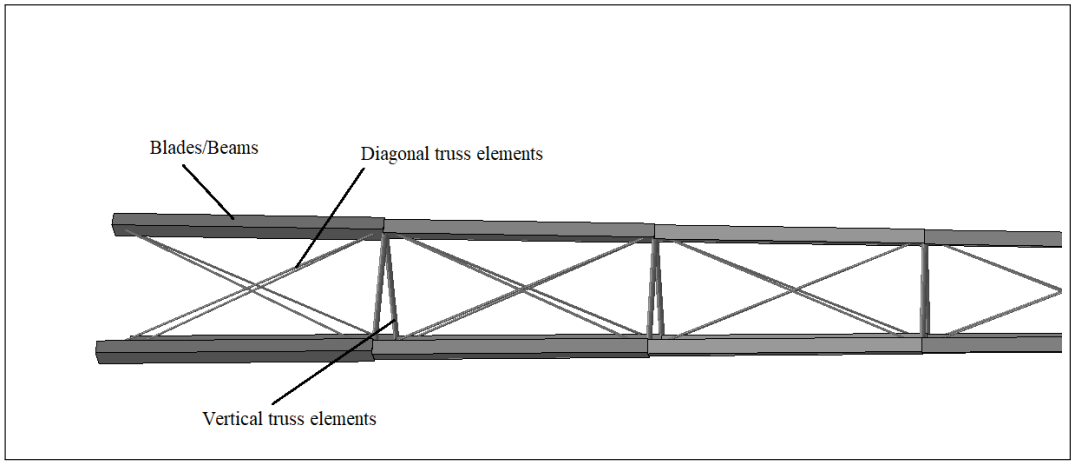

Figure 2.1: Part of the Triblade design with notations of main components.

2.1.1 Aerodynamic design and load cases

The main objective of a wind turbine is to transform wind energy acting on the turbine blades to kinematic energy that in turn produces electricity. The turbine must then be constructed in such a way that wind generates forces tangent to the rotation of the blades. This is done by means of airfoils. The airfoil shape is able to produce lift when moving through a fluid. This property has been utilized in many different applications, such as airplanes, propellers, hydrofoils and many more. See figure 2.5 for the general shape of a foil.

When designing a wind turbine two major types of load cases are considered; the production load, where the blades are spinning allowing the generator to produce energy, and the the stand still load case. The production load case will generate loads proportional to the effective velocity vectors of the wind and the blade.

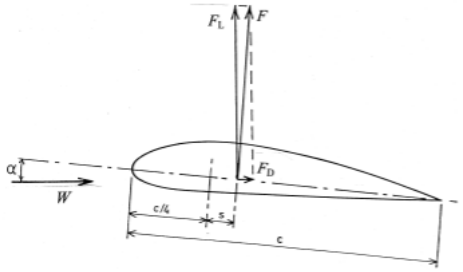

Figure 2.2: Illustration of the effective wind velocity used for load calculations. Det Norske Veritas, 2002

The effective wind velocity, see figure 2.2 is the velocity of the wind relative to the velocity of the blade.The resulting wind velocity is calculated as the sum of the relative velocities of the blade and the wind. The wind velocity from the production load case is considered when calculating the rotations of the blades.

$$v_{eff} = \sqrt{v_r^2 + v_w^2}$$

Where v_{eff} is the effective wind velocity, v_r is the tangential velocity of the blade section and v_w is the wind velocity The resulting forces from the wind are shown in figure 2.2. The lifting force is thus generated by the difference by the difference in velocity of the upper and lower air flows (Det Norske Veritas, 2002).

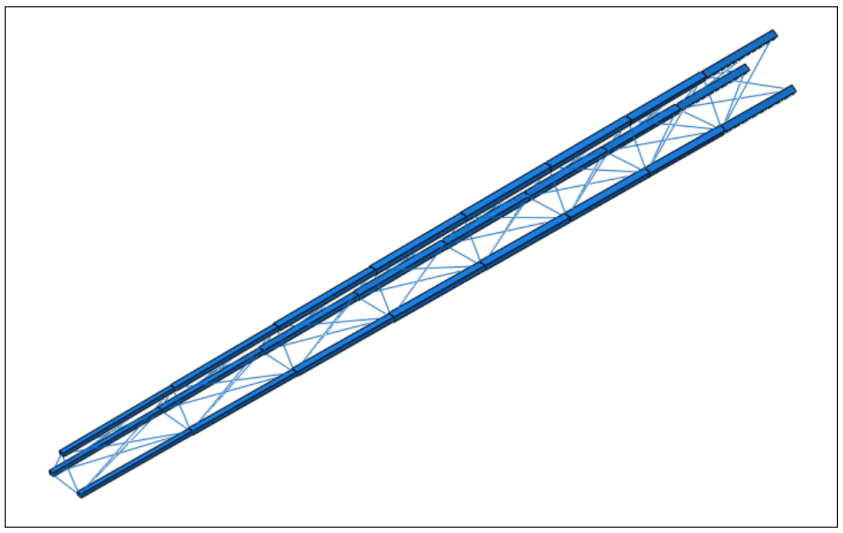

Figure 2.3: Model of the Triblade done in Abaqus/CAE

The stand still load case, which will be the focus of this thesis, refers to the scenario where the turbine has been shut down due to excessive wind speeds.

The turbine blades need to be able to withstand wind velocities up to 60 m/s in any direction. The most unfavourable wind direction is when the wind is blowing directly perpendicular to the blade's rotational plane, i.e. the Y-direction as defined in figure 2.4. The moment induced by the wind must be resisted through compression and tension of the beams in the truss network, and this case results in only one of the beam lines being subjected to compressing forces.

The resulting force on the blade is calculated with the following formula

$$F_{dA} = \rho v^2 c_d \cdot CL$$

Where ρ is the density of the air, v is the wind speed, CL is the Chord length and $c_d = 1.17$ is the coefficient of drag.

Besides the obvious loads generated from the wind there are two other loads acting on the structure, the self weight of the structure and the centrifugal force generated from the rotation during production.

While considering the stand still load case those loads will not be considered as the blades are not rotating and therefore are not generating any centrifugal forces. The weight of the structure will not coincide with the wind direction that will be the most unfavorable, but it can still increase the stresses.

2.1.2 Structural design

While a traditional wind turbine blade is constructed in one piece, and acts as a single beam, the Triblade design instead utilizes a truss system, and is thus composed of multiple structural members. The truss system in the Triblade is thus composed three types of members:

- The beams which run horizontally along the structure, and constitute the main load bearing components of the Triblade. It is also one of three blades in the structure around which the airfoils are swept. The beams resist loads via tension, compression and bending depending on the loadcase.
- The diagonal bars, which serve to distribute loads between the beams and enable them to work in conjunction. Due to their slenderness, the diagonals are only able to carry tension forces. They will also enable pre-tensioning of the truss system.
- The vertical bars, which serve to keep the distance betweem the beams. The verticals will therefore mostly carry forces in compression.

The Triblade is divided into eight sections (see figure 2.3) to simplify the erection process and transportation while also giving extra stability and load bearing capacity to the blade.

Each section is comprised of three beams, six diagonal bars in pretension and six vertical bars. In this report, the beams in each section and the entire rows of beams will be referred to as A, B and C, according to figure 2.4

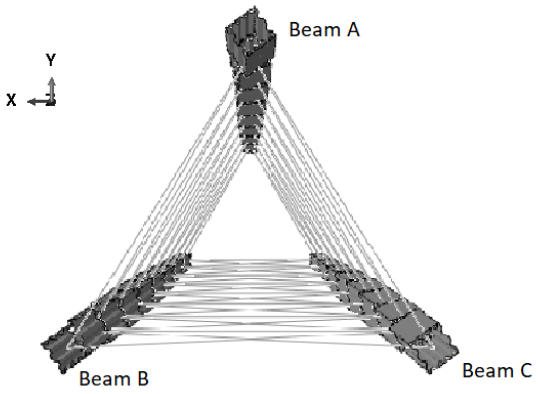

Figure 2.4: Labeling of beams in the structure.

The most important part of the Triblade is the airfoils which generate the lift required to produce energy. The airfoil will be constructed using either carbon fibre reinforced polymer (CFPR) or glass fibre reinforced polymer (GFPR) is are swept around a load bearing beam constructed in steel. As the foil has the purpose of generating the lift needed to produce energy the beam has mainly a structural purpose by transferring the loads generated from the wind. For future reference, the following terminology considering the structural parts of the airfoil is helpful, see also figure 2.5:

- Airfoil - The cross sectional shape of the blade.
- Chord line - The shortest line between nose and tail of the airfoil.
- Spar cap - The flanges of the load carrying beam.
- Shear web - The web of the load carrying beam.
- Shell panel - The panel that makes up the surface of the airfoil.

Analogous to a regular beam, the spar caps (flanges) resist normal forces and the shear webs resist shear force. The airfoils are constructed using GFRP and CFRP, while the beams were investigated to med made of steel.

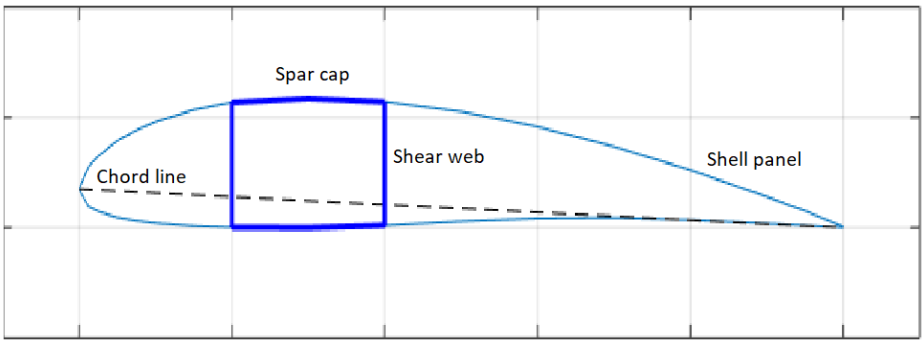

Figure 2.5: Sketch showing an airfoil with the different components denoted.

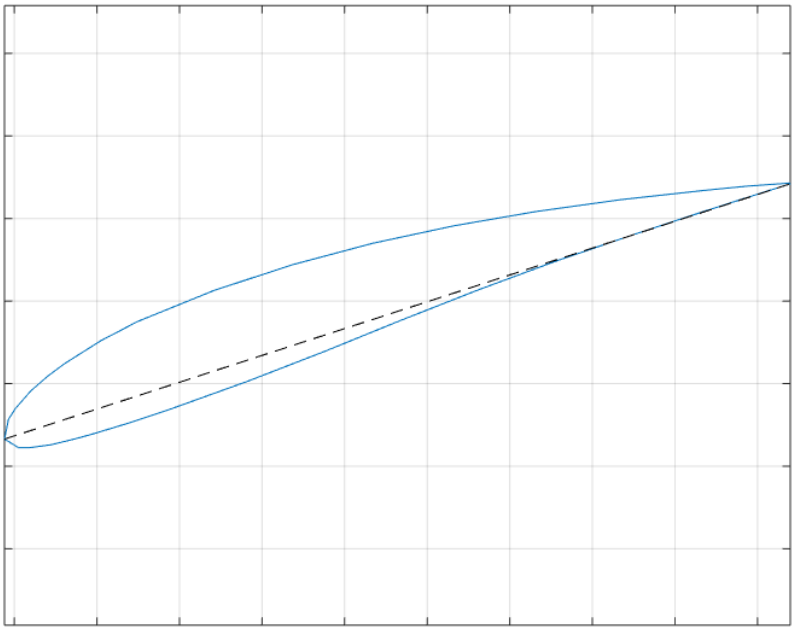

Figure 2.6: Sketch showing the rotation of the foil

The blades are discretely rotated about its length (roughly in the direction of the Z-axis in figure 2.4) where the chord line is rotated an angle (β) to optimize lift considering the angle of attack from the effective wind.

$$\boldsymbol{\beta} = [-35.75°,\ -18.28°,\ -9.24°,\ -4.55°,\ -2.35°,\ -0.99°,\ 0.26°,\ 2.59°]$$

Each section has six diagonal bars and six vertical bars. These enable the transfer of forces between the beams, and will be henceforth referred to as diagonals and verticals. The diagonals are pretensioned in order to counteract deflections. The diagonals and verticals were investigated using steel. In practice, both diagonals and verticals will be covered in neutral airfoils to reduce drag. The diagonals are very slender, and can be assumed to only carry loads in tension.

2.2 Materials in turbine blades

The material choice is important when designing wind turbine blades and the most important factors to consider are a high stiffness/density ratio and a long fatigue life.

A high material stiffness is important to preserve the aerodynamic performance during high winds. A high material stiffness will also allow for more slender elements in the blade and resulting in reduced volume of the structure and then also the weight.

A low density ensures a higher degree of efficiency while also reducing the moment that will have to be resisted at the nave during stand still conditions due to gravity. However, problems with buckling increase with increasing slenderness.

The dynamic nature of wind presents a need for a material with a long fatigue life. A wind turbine with an expected lifetime of 20 years may be subjected about 10^7 equivalent load cycles. Fatigue is, however, not that essential to consider while designing for the stand still load case that are expected to occur one or two times in the designed blade lifetime.

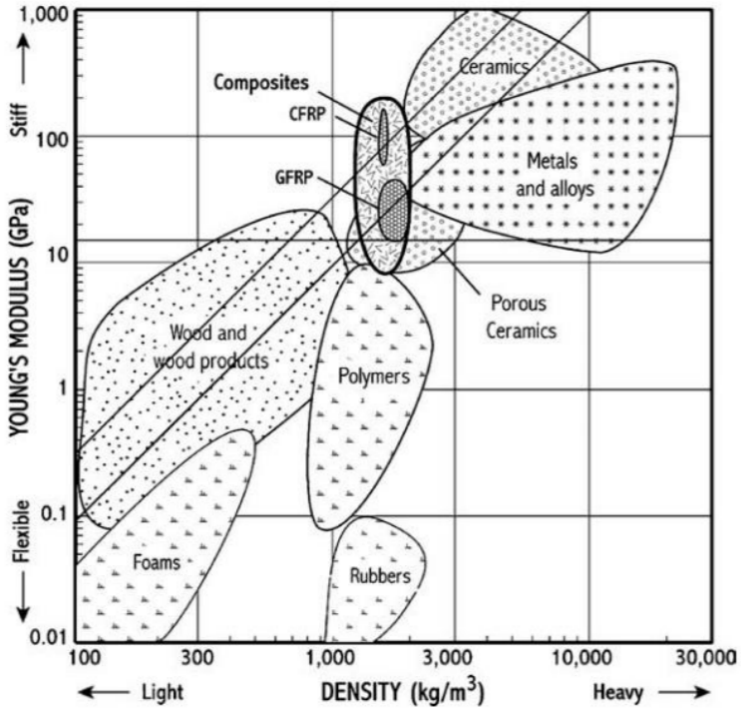

Figure 2.7: Stiffness-density ratio of a selection of materials (Brøndsted et al., 2005)

Considering the aforementioned material requirements both carbon fibre reinforced polymer (CFRP) and glass fibre reinforced polymers (GFRP) are the most suitable materials and are therefore, the two materials mainly used in conventional blades. These materials are, however, expensive compared to steel, which also has a relative high stiffness/density ratio. Another factor to consider when using steel instead of fibre reinforced polymers is that the yield strength is significantly lower even if high grade steel is used (Brøndsted et al., 2005).

Material	Young's modulus E, [GPa]	Tensile strength σ_{yield}, [MPa]	Density ρ, [kg/m^3]
GFRP	38	1800	1870
CFRP	176	2050	1490
Steel	210	500	7800

Table 2.1: Material properties (Wadsö, 2015)

In this thesis, steel is investigated as the main structural material in the beams, diagonals and verticals. The advantages of steel, aside from its higher stiffness when compared to composite materials, is mainly cost-related. Steel is considerably cheaper than GFRP's and CFRP's, and would greatly reduce production costs if it could be used.

3 Theory

This section will give a summary of the theory that the thesis is based on, and will conceptually cover the finite element method as well as linear and non-linear buckling.

3.1 The finite element method

In engineering mechanics, many problems consist of solving partial differential equations (PDE's). This applies to problems such as heat flow, structural analysis, mass transport and electromagnetic potential, to name a few. For many complex problems, the PDE cannot be solved analytically. In these cases, the finite element method (FEM), a powerful numerical tool, may be used to approximate the solution of the problem over a given region. There are a number of commercial FEM-programs available today. In this thesis, ABAQUS CAE, a program developed by Dassault Systèmes, is used.

When performing finite element analysis (FEA), one divides the region into several individual *elements*. Each element is assigned *nodes*, points often located on the boundary of the element, at which the quantity of interest is evaluated, such as displacement or temperature. The values at the nodes are the unknowns for which to solve, and the values over the element may then be interpolated using *shape functions*. The problem may be 1, 2 or 3-dimensional, and depending on the type of problem the values at the nodes will vary depending on direction. Each node is therefore assigned *degrees of freedom* (DOF's). For a general 3D problem where displacement is studied, each node will then have 6 DOF's: displacement along the x, y and z-axes, along with a rotation about each.

The collection of elements over the region is called a *mesh*. In practice, a problem will typically consist of multiple elements (often on the scale of millions). The mesh is directly related to the computational cost, where a more coarse mesh reduces the computational but reduces the accuracy of the results. This will result in a system of equations, which may be conveniently expressed in matrix notation. For a general static problem, this may be written as

$$\boldsymbol{K}\boldsymbol{u} = \boldsymbol{f_l} + \boldsymbol{f_b}$$

Where $\boldsymbol{K}$ is the system's stiffness matrix, $\boldsymbol{u}$ is a vector containing the displacement at the nodes and $\boldsymbol{f_l}$ and $\boldsymbol{f_b}$ are vectors containing loads acting on the nodes over the body and at the boundaries, respectively (Ottosen, 1992). In order to solve the system, boundary conditions are required, i.e. points at which the initial displacement and/or forces are known (e.g. zero displacement and rotation at the support of a pinned cantilever beam). The solution approaches the exact solution for an increasing amount of elements. For a comprehensive introduction to the finite element method, the textbook *Introduction to the finite element method* (Ottosen, 1992) is recommended.

3.1.1 Element types

There are many different types of elements which may be used in an analysis. Here, only the elements used in the thesis will be described, these are truss, beam and shell elements.

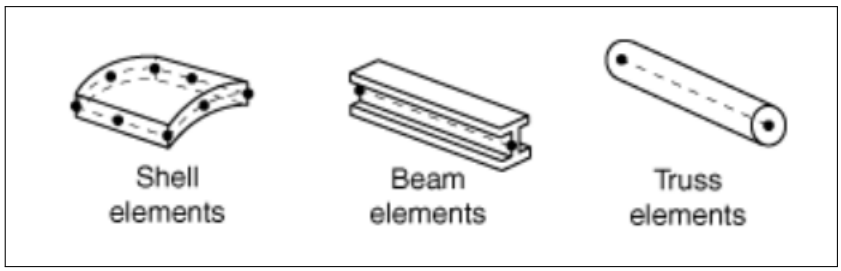

Figure 3.1: Element types used in the model (Dassault Systèmes, 2015).

Shell elements

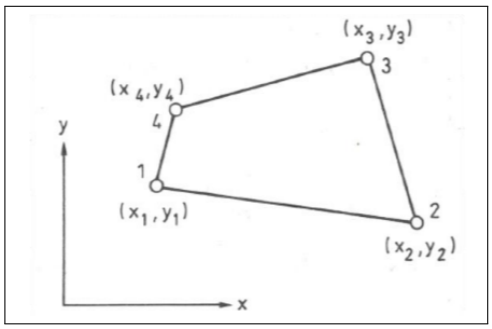

Figure 3.2: Quadrilateral element used to mesh the shell elements (Dassault Systèmes, 2015).

A shell element is a surface element, and is useful when modeling structural components where the surface area is large in relation to thickness. With stiffness in all three dimensions, the shell element is capable of transferring load both in and out of plane. The stiffness of the shell is dependent on it's assigned thickness and material properties. The element is based on plate and membrane theory, and may in certain situations be superior to 3D-solid elements, due to the lower number of DOF's and the lower computational cost. The elements used in this analysis are quadrilateral elements with 4 nodes. Each node has three translational and two rotational DOF's. The translational DOF's are along the x, y and z-axes, while the rotational DOF's are only located about the x and y-axes, see figure 3.2.

Beam elements

A beam element is a linear element with nodes at either end and may contain more nodes in between, depending on if one assumes linear, quadratic or an even higher order of geometry. The beam elements used in this analysis use 2 nodes and 12 DOF's, see figure 3.3. Due

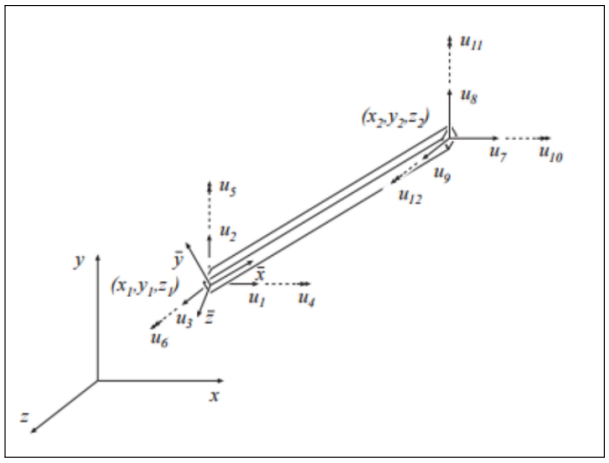

Figure 3.3: 3d Beam element.(Dassault Systèmes, 2015)

to it's rotational stiffness, the beam element may carry load through bending, in addition to compression and tension.

Truss/bar elements

The truss/bar element is a linear element which has no rotational stiffness. As such, it may only resist loads via either compression or tension. The elements used in this analysis use 2 nodes and 6 DOF's. In addition, the elements can be assigned zero stiffness when in compression (Ottosen, 1992).

3.2 Buckling

Buckling is a phenomenon where the failure mode is determined by stiffness of the structure instead of the yield limit. This section will give a theoretical background to the buckling phenomenon.

3.2.1 Linear buckling

Linear buckling, also called Eigenvalue buckling, predicts the theoretical buckling strength of an ideal elastic structure. For an eigenvalue buckling analysis of a column corresponds to the classical Euler solution which is derived bellow.

The first step in the Euler beam case is to identify the internal moment $M = -P \cdot y$ where P is the axial pressure and y is the beam deflection. By inserting the above mentioned expression in the formula for beam-bending $M = EI \cdot y''$ the differential equation is given as

$$EI \cdot y'' = M = -P \cdot y \tag{3.1}$$

The solution to the differential equation is given as

$$y = A \cdot \sin\left(\sqrt{\frac{P}{EI}}\right) + B \cdot \cos\left(\sqrt{\frac{P}{EI}}\right) \tag{3.2}$$

Where A and B are constants depending on the boundary conditions. (*Column buckling*)

3.2.2 Nonlinear buckling

The analysis of plates or shells using the finite element method in this thesis includes solving large systems of nonlinear equations. The non-linearities are a consequence of for example the large deformations or nonlinear material properties that alters the structure with respect to geometry and stiffness of the structure. For nonlinear buckling problems the structural properties needs to be continuously updated throughout the solving and are further discussed in chapter 4. The deformations from the finite element formulation can be described as with n-number of deformation parameters. Solving the equilibrium equations for small steps either of load or deformation gives the equilibrium path also known as a load-deformation curve.

The newton-Raphson method is an iterative solving method (se figure 3.5) , in which the total load is applied in a number of smaller steps. For each load step, the solver will iterate until equilibrium is fulfilled. This is done when the energy residual reaches below a certain threshold. When equilibrium is fulfilled it is accepted as the true solution and the next load increment is applied.

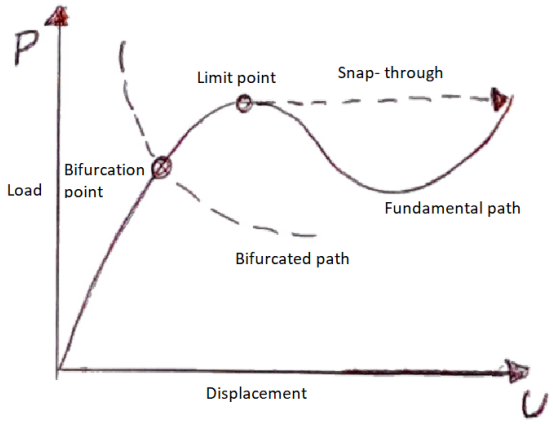

Figure 3.4: Schematic presentation of an equilibrium path with critical points

There are different variations of the Newton-Raphson scheme, where the full Newton-Raphson method updates the tangential stiffness used to solve the next equilibrium point while the modified Newton-Raphson method uses the tangential stiffness of the initial state for all calculations.The full Newton-Raphson usually has a faster convergence rate but with a higher computational cost compared to the modified Newton-Raphson. By default ABAQUS uses the full Newton-Raphson scheme but has options regarding the rate of update of the tangential stiffness used (Ristinmaa, 2018).

For analyses containing a complex load distribution, a load pattern is established in order to apply the loading equally all over the body. The load pattern is initially defined as a normalized force vector, with the loads at the individual DOF's normalized to a value between 1.0 and -1.0, depending on their true magnitude and direction. The vector is then multiplied by a scalar in steps. When equilibrium is achieved, the scalar is increased and the next step is initiated. The process is repeated until either the load has been fully applied or the solution fails to converge.

The degree of loading where buckling occurs presents themselves as bifurcation points for numerical solving methods. At the bifurcation point, the static equilibrium can follow multiple paths for an increasing load, a purely compressed state or a lateral-deformed state, i.e. buckling. To trigger the secondary path, small transverse loads can trigger the lateral-deformed state. Transverse loading or initial deformations are good ways to model imperfections from e.g. oblique loading, initial deformations of the structure or material imperfections (Riks, 1979).

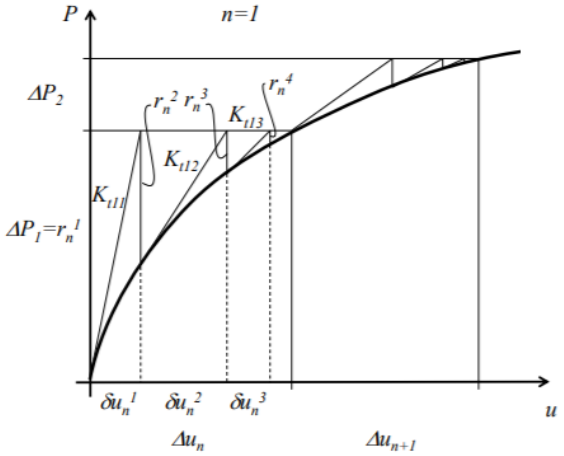

Figure 3.5: Full Newton-Raphson iteration scheme Persson, 2018

Full Newton-Raphson scheme

Initiate quantities

$\boldsymbol{a}_0$; $\boldsymbol{\varepsilon}_0$; $\boldsymbol{\sigma}_0$; $\boldsymbol{f}_0$; $\boldsymbol{f}_{int}$;

For loadstep $n = 0, 1, 2, \ldots N_{max}$

Determine new load level f_{n+1}

Initiation of iteration quantities

$\boldsymbol{a}^0 = \boldsymbol{a}_n$

Iterate $i = 1, 2\ldots$ until $|\psi|_{norm} = |\boldsymbol{f}_{n+1} - \boldsymbol{f}_{int}|_{norm} < tol$

Calculate stiffness $\boldsymbol{K}_t = \int_V \left(\boldsymbol{B}^T \boldsymbol{D}_t^{\,i} \boldsymbol{B}\right) dV$

Calculate displacement $\boldsymbol{a}^i$ from $\boldsymbol{K_t}\left(\boldsymbol{a}^i - \boldsymbol{a}^{i-1}\right) = \boldsymbol{f_{n+1}} - \boldsymbol{f_{int}}$

Calculate strain $\boldsymbol{\varepsilon}^{\boldsymbol{i}} = \boldsymbol{B}\boldsymbol{a}^{\boldsymbol{i}}$

Determine stress $\boldsymbol{\sigma}^{\boldsymbol{i}}$ from constitutive equations

Calculate internal forces $\boldsymbol{f_{int}} = \int_V \left(\boldsymbol{B}^T \boldsymbol{\sigma}^i\right) dV$

End iteration loop

Accept quantities

$\boldsymbol{a}_{n+1} = \boldsymbol{a}^{\boldsymbol{i}}$; $\boldsymbol{\varepsilon}_{n+1} = \boldsymbol{\varepsilon}^{\boldsymbol{i}}$; $\boldsymbol{\sigma}_{n+1} = \boldsymbol{\sigma}^{\boldsymbol{i}}$; $\boldsymbol{f}_{int}$

End load step loop

4 Finite element model

The finite element model is the foundation of the analysis in this thesis. In this thesis Abaqus/CAE was used to create the model, solve the simulations as well as in evaluating the results. To simplify the procedure of conducting parametric studies a Python script was created for both generating the models and extracting relevant results from the analysis.

In this chapter the process of developing the model from data and design provided by Winfoor, including modeling techniques, simplifications and assumptions are presented.

4.1 Terminology and components of the model

4.1.1 Terminology

In this chapter, the following terminology will be used:

1. *Part*
    - An ABAQUS part is a discrete component of the structure to be analyzed. A part is initially defined by it's geometry. Further, the part may be defined by certain characteristics which will later impact the way the part is meshed. A part may for instance be defined as a solid, a shell, a line, and a number of other options. In this thesis, the part types used are lines and shells.
2. *Shell structure*
    - A shell is a type of part geometry, characterized by it's 2-dimensional nature. A shell is in essence a 2-D plane, which may be flat or curved. In this thesis, 2-D shell elements are used in order to construct the various types of cross-sectional types to be analyzed. A part defined by shell tructures will later on be restricted to using shell elements.
3. *Line*
    - A line is a type of part geometry. It is defined as a simple 1-D line in 3-D space. A part defined as a line will later on be restricted to using either beam or truss elements. A very slender structural component may be modelled using parts defined by lines, and in this thesis the diagonals and verticals are defined as such.

4. *Section*

    - In ABAQUS, a section is a collection of properties assigned to a part. A section must defined for a type of geometry, e.g. shells or lines, and contains material properties. Taking a shell part as an example, the section will be defined as a shell section, where the user must define the shell thickness (i.e. the thickness of shear and spar caps in this case) and which material the shell consists of. The material properties, including elastic, plastic and thermal characteristics, are defined separately in the material module (Dassault Systèmes, 2015).

5. *Module*

    - An ABAQUS module is an instance of the program where a certain aspect of the model is treated. Examples of modules are; the part module, where parts are created, the material module, where materials are defined and the mesh module, where the the model is assigned an element mesh.

6. *Assembly*

    - In the assembly module, all parts of the model are assembled into the global structure. The structure defined in assembly is later used when when defining constraints in the model, i.e. how various parts (structural members) interact with one-another.

7. *Constraint*

    - A constraint is a geometric restriction used in the assembly module, and is used to define the position of a part in 3D-space. This may be with respect to other parts or datums (points of reference) defined in 3D-space.

8. *Interaction*

    - Interactions define how various parts interact with each other. This means defining which degrees of freedom are shared between parts. This may be used to define e.g. a weld between two structural components.

The structure consists of three main types of components, these are the *beams* (around which the airfoils are swept) and the diagonal and vertical *bars*. Since the scope of this thesis is restricted to determining a sufficient cross sectional type, the air foils themselves are not modelled. Additionally, steel plates are placed along corrugations of the beam. This is intended to provide some extra stability, and may be a viable option when designing the connections between beams and foils in practice. The steel plates also serve the purpose of providing an easily defined surface when applying the various loads, discussed further in chapter 4.5. How the various structural members are modelled is described below.

4.1.2 Structural components

The beams consist of steel shell sections, and are as such restricted to the shell element type. The steel was assigned either purely elastic or elastoplastic properties depending on the analysis type, see chapter 4.3.

A number of shapes of the cross sections needed to be analyzed globally. Due to this need, the script was written in such a way that any cross section which may be characterized as a polygon made up of straight lines could be analyzed, see figure 4.1. The beams are then

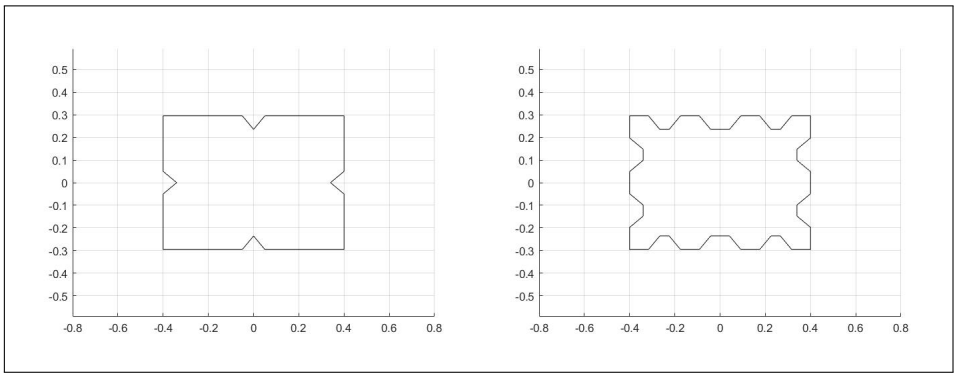

Figure 4.1: Examples of cross sections generated by an external script which are compatible with the main script.

generated by extruding the defined cross section to the desired length of the beam.

The beams may be created by any input file which generates a coordinate matrix in which the n vertices (x_i, y_i) of the the defining polygon are contained. The matrix must be in the format below:

$$\boldsymbol{Coord} = \begin{bmatrix} x_1 & y_1 \\ x_2 & y_2 \\ \vdots & \vdots \\ x_n & y_n \end{bmatrix}$$

The beams were defined by an input file which generated a coordinate matrix for the desired cross sectional type for beams A1, B1 and C1, see figure 4.2 Beams A2-8, B2-8 and C2-8 were then generated by scaling beam 1 in each row by a certain factor.

The thickness of the beams was also calculated in the input file. This was accomplished by requiring that beams A1, B1 and C1 should weigh the same as a reference beam. The reference beam was of a simple rectangular shape, with dimensions WxH: 800x591mm, and a thickness of 10mm in the shear web and spar caps. The thicknesses of beams 2-8 in rows A, B and C were then defined by scaling down the thicknesses of beam 1. Further, the thickness was defined as constant over the entire cross section.

The plates were modelled using shell parts, and are therefore also restricted to using the shell/plate element type. The plates were also modelled with respect to the coordinates generated for the beams. The plate sections are defined as 2mm thick shell sections, with the same material properties as the steel beams.

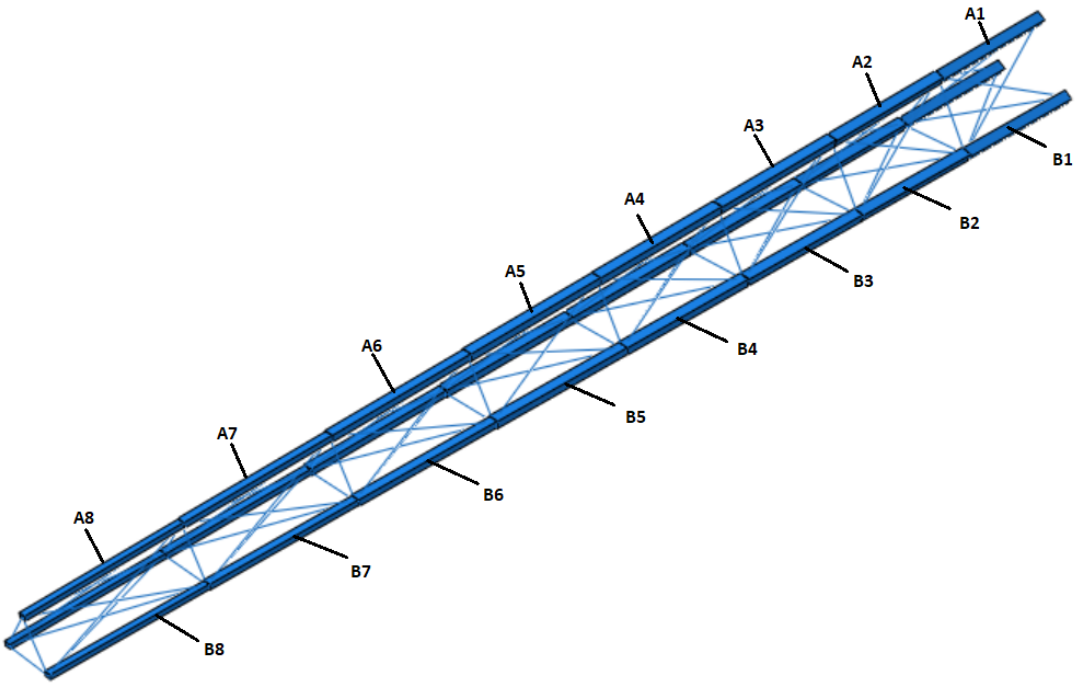

Figure 4.2: Enumeration of the beams. Beams C are not listed but are on the far side of the rendering and follow the same numbering system as A and B.

The diagonals and verticals were modelled using line parts, which later restricts them to being meshed by either beam or bar elements. Additionally, the diagonals were assigned the *No Compression* property. This means that the stiffness is reduced to zero if these members are subjected to compression forces. Due to restrictions in ABAQUS, this means that these members may not be assigned plastic material properties. The diagonals are also subjected to prestress loads, which was modelled using thermal loads in ABAQUS. The properties defined to model this are discussed further in chapter 4.5.

4.1.3 Initial dimensions of components

The initial dimensions used in the various types of analyses are given in the tables below.

Section	Area [mm^2]
1	1613
2	2075
3	1602
4	1297
5	935
6	610
7	340
8	88

Table 4.1: Cross sectional area of diagonals in each section.

Triangle	**Area [mm^2]**
1	-
2	12240
3	12240
4	12240
5	12240
6	11020
7	8064
8	5992
9	4416

Table 4.2: Dimensions for verticals

The cross sections generated for the model are displayed in figure 5.8 in chapter 5.3.

The dimensions WxH are scaled relative to the width in beam 1 in each row A, B and C, in the same manner as the chord length CL. I.e., $w_i = w_1 \cdot (CL_i/CL_1)$. See table 4.3 for initial given dimensions.

4.2 Interactions & constraints

Three types of interactions were used to model the various connections in the structure. Two types of multipoint constraints (MPC's) were used, along with *Tie* constraints. The types used were *MPC Pin* and *MPC Beam*. MPC constraints use two defined node regions, a master and a slave region. The slave regions DOF's are set equal to those of the master region, meaning that the slave nodes and their DOF's are eliminated from the calculations, and the connection is completely dominated by the master region. An *MPC Pin* constraint sets all translations of the slave region equal to those of the master, while still allowing for independent rotation, i.e. all translational DOF's are set equal. An *MPC Beam* constraint sets all DOF's equal, i.e. the slave region will mirror any response in the master region. *Tie constraints* are defined between two surfaces, and also make use of a master and a slave surface. This sets the DOF's of the slave surface equal to those of the master surface throughout the entire duration of the simulation

The connections between the beams, veritcals and diagonals at their junctions were modelled as MPC's. The two MPC's used were *MPC Beam* and *MPC Pin*. *MPC Beam* ties all DOF's for the coupled nodes, i.e. they share all translation and rotation. *MPC Pin* couples all translational movement between two nodes, while allowing for individual rotations in all dimensions. The connection between the beams and the foils (modelled as individual plates

Section 1	Section 2	Section 3	Section 4	Section 5	Section 6	Section 7	Section 8
800x591	800x591	800x519	800x591	755x558	659x487	557x412	478x353

Table 4.3: Dimensions of the beams [WxH] for each section in mm.

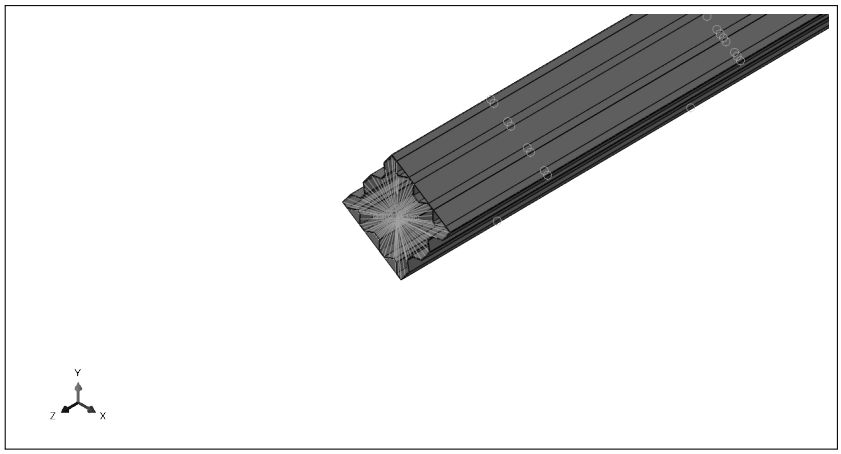

Figure 4.3: Constraints for a single beam.

connected to the lower and top spar caps) were modelled using the *Tie* interaction between the beam and plate surfaces. Partitions matching the corrugation pattern of the beams were created on the plate surfaces in order to ensure 1 to 1 coupling of the DOF's.

The model geometry was defined using a set of coordinates specifying the position of all beam center-line-ends in 3D-space. At each coordinate, a reference point (RP) was generated. These serve as the master nodes in the MPC constraints. Each beam was constrained to these RP's at either end, see figure 4.3, with the edges at the beam ends serving as slave node regions.

The verticals and diagonals were constrained at the same points as the beams. Here, a simplification was made. In practice, the actual joint will have to be placed offset from the beams central axis. The forces acting in the diagonals will therefore give rise to torque about the RP, which will be resisted by the beams, see figure 4.4. Due to the exact design of the joints being unknown at the time of the thesis, the decision was made to constrain all components in the center line of the beams. The joints were modelled using *MPC Pin*, allowing independent rotation of both verticals and diagonals, see figure 4.5. When modelling the connection at the nave, *MPC Beam* constraints were used, coupling all DOF's along the beam cross section edges to a central reference point. This is presented in section 4.4.

The plate and beam sections in the blades where tied together using the TIE constraint. Since the nodes on the edge of the beam where already used as slave nodes the plates where put as the slave surface.

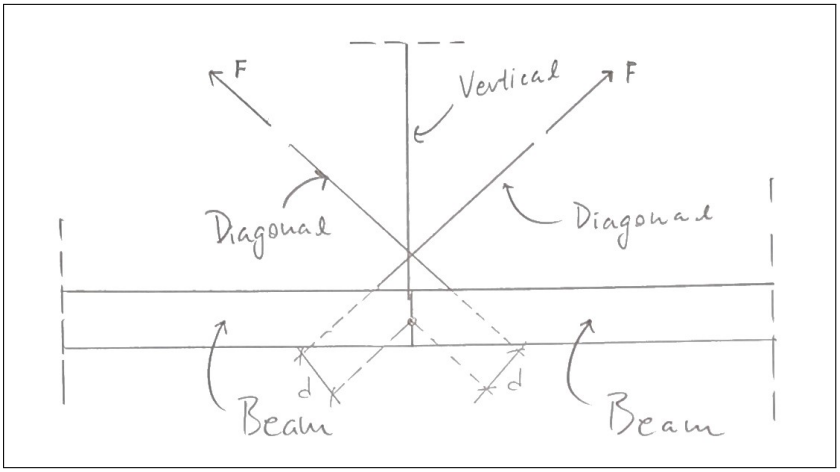

Figure 4.4: Principal sketch showing the modelling of joints. The leverarms d will induce moments in the connection due to the forces F.

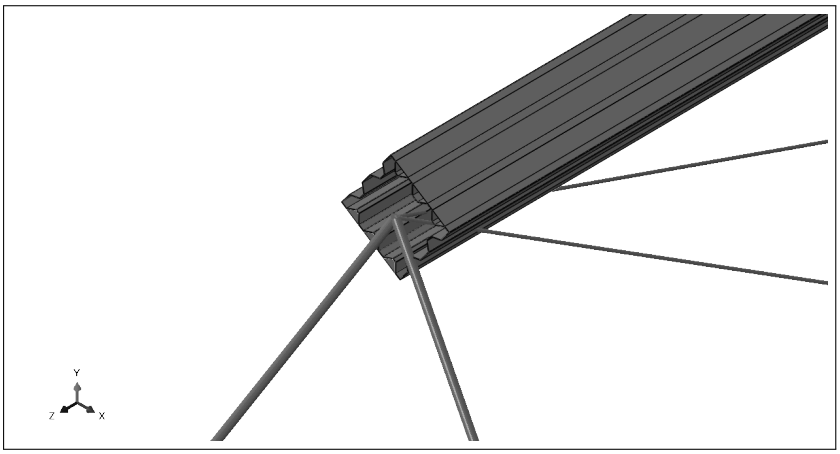

Figure 4.5: A cut of the model, showing the joints with profiles and shell thicknesses rendered.

4.3 Material

It is possible to define the materials used in the beams, diagonals and verticals separately. In this thesis however, steel with the properties presented in table 2.1 are used. For all sections except the diagonals, the steel was defined with elasto-plastic properties. This was a consequence of plastic properties not being applicable to elements using the $NoCompression$ property. For simplification, the stress-strain curve of the steel was assumed as ideal elastic-plastic, as shown in figure 4.6.

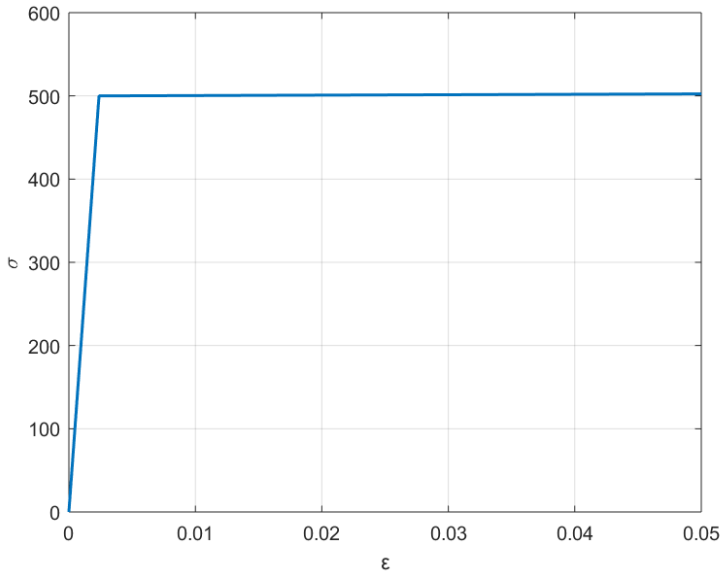

Figure 4.6: Idealized stress-strain curve.

4.4 Boundary conditions

To model the boundary conditions at the root of the beam edges at the blade root were tied with *MPC beam* connections to a nave reference point (se figure 4.7) to which the boundary conditions where applied. The boundary conditions prescribes all translation and rotation of the reference point.

Additionally, the possibility of having the beams hinged about the x-axis was investigated, see figure 4.8. This BC is analogous to the types of connections at the foundations found in e.g. two and three hinged arch bridges.

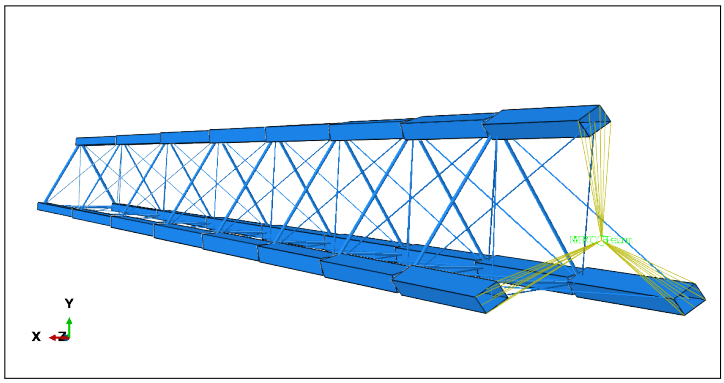

Figure 4.7: The boundary condition shown with the MPC constraints from the beams to the nave point.

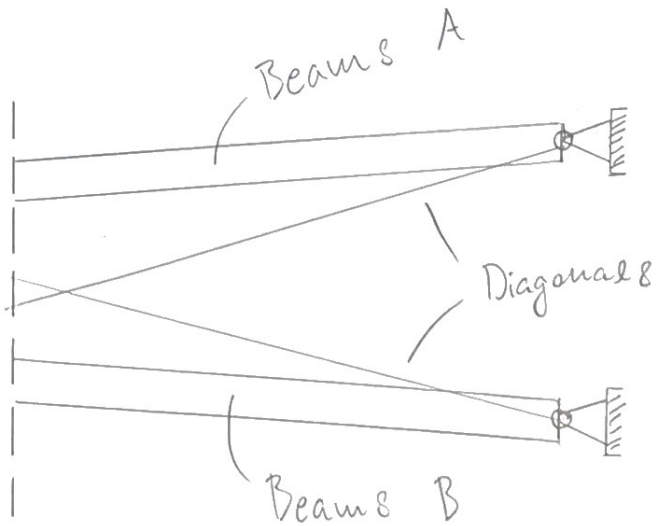

Figure 4.8: Hinged connections

4.5 Loads

The structure is subjected to wind loads, which also give rise to torque in the beams as a result of the beam center lines not coinciding with the rotational center of the airfoils. Additionally, the diagonal members are prestressed in order to reduce deformations. In this chapter, the modelling of the wind load and prestress loads with assumptions are presented.

4.5.1 Static traction load and torque

The Static load from the stand still load case was modelled as a surface traction placed on the top and bottom plates to eliminate moments due to uneven loading. The load direction was the same for all the beams, acting purely in the y-direction in the model coordinate system, see figure 4.9.

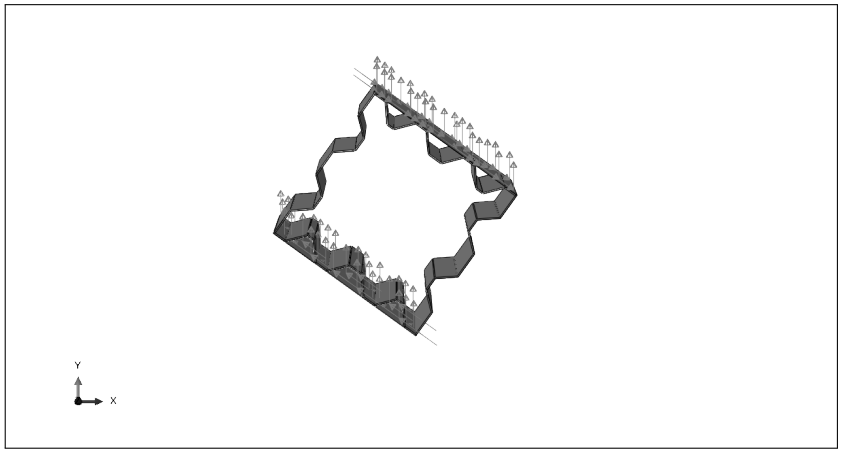

Figure 4.9: Figure the load application on the plate sections of the beam.

As a consequence of non-centered placement of the bearing beam in the airfoil a continuous torque will act on the beams. The center line of the beams was assumed to to have a distance 20% of the chord length from the center of the foil. The torque was modelled as a force couple from surface traction loads applied to the bottom and top plate of the beams, see figure 4.9, which resulted in a torque about the beams local z-axis (right-hand-rule with the local z-axis pointing roughly in the direction of the global z-axis).

The static windload may be calculated for each section with a chord length $\boldsymbol{CL}_i$, where

$$\boldsymbol{CL} = [6/3 \;\; 6/3 \;\; 6/3 \;\; 6/3 \;\; 5.6602/3 \;\; 4.9392/3 \;\; 4.1792/3 \;\; 3.5812/3]$$

The windload acting on a single airfoil in a section i is given as

$$F_{d,i} = \frac{1}{2}\rho c_d v^2 A_i$$

where $A_i = (CL)_i L_i$, and the beam length $L_i = 11.254$m for each section, the resulting loads for each section were calculated:

$$\begin{aligned}\boldsymbol{F}_d &= 1.4224 \cdot 1.17 \cdot 60^2 \cdot [6/3 \;\; 6/3 \;\; 6/3 \;\; 6/3 \;\; 5.660/3 \;\; 4.939/3 \;\; 4.179/3 \;\; 3.581/3] \cdot 11.254 \\ &= [58068 \;\; 58068 \;\; 58068 \;\; 58068 \;\; 54779 \;\; 47801 \;\; 40446 \;\; 34658] \text{ N}\end{aligned}$$

The surface traction will then depend on the length and width of the spar caps in beam type used in the global model. The surface traction was then calculated for each beam and section as:

$$\sigma_i = \frac{F_{d,i}}{2b_i L_i}$$

Where b_i and L_i is the width and length of beam i, and the factor two in the denominator serves to split the load equally between the upper and lower spar caps.

The static wind will generate torque due to the fact that the rotational axices of the beam and the foil do not coincide. The torque was approximated according to figure 4.10.

The torque in any section i may then be calculated as

$$T_i = 0.2F_{d,i}(CL)_i$$

The torque along the sections is given in the vector $\boldsymbol{T}$ below.

$$\boldsymbol{T} = [23227 \;\; 23227 \;\; 23227 \;\; 23227 \;\; 20671 \;\; 15740 \;\; 11269 \;\; 8275] \text{ Nm}$$

Since the torque is to be modelled as a surface traction, split evenly between the top and bottom spar cap plates, the following must hold:

$$2\sigma_i A_i \frac{h_i}{2} = T_i \;\Rightarrow\; \sigma_i = \frac{T_i}{A_i h_i}$$

where A_i and h_i are the area of the plates and height of beam i, respectively.

4.5.2 Preload

The preloading of the diagonals was modelled using predefined temperature fields. To model this, the bars material properties were given a thermal expansion coefficient proportional to

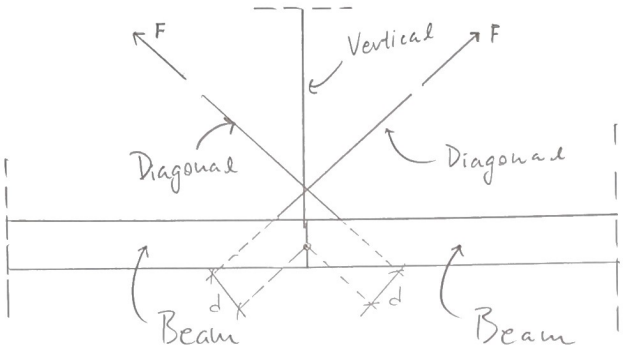

Figure 4.10: Torque simplification with the airfoil is simplified as a rectangular plate.

the diagonal area and stiffness.

$$\sigma = E\varepsilon$$
$$\Delta L = \alpha \Delta T L$$
$$\varepsilon = \alpha \Delta T$$
$$\sigma / E = \alpha \Delta T$$
$$\alpha = A/E \Rightarrow F = \Delta T$$

By defining α as a ratio depending on the cross section and material properties, it is easy to define the preload. The predefined fields where done by applying a temperature to each of the diagonal elements with a magnitude equal to that of the intended preload, see table 4.4. This done in an iterative process until the desired preload was achieved.

Section	Preload [kN]
1	20
2	20
3	20
4	20
5	15
6	10
7	8
8	8

Table 4.4: Preload of the diagonals

The preload was applied in a separate step were only the temperature loads (pretension) were applied. This was done simply to ensure that the preloads were applied as intended.

5 Numerical studies

This chapter will present the results from the parametric studies and also the most beneficial cross sections considering the bearing capacity as well as weight.

5.1 Analysis procedure and data extraction

The full simulation consisted of two separate analyses, a buckle analysis and a general static analysis with regard to non linear geometry and plastic behaviour. Both analyses are further divided into two steps.

In the first step, the temperature (preload) is applied to the diagonals in each section. Here, the von Mises stress is extracted and used to calculate the maximum tensile force acting on any diagonal in each section. The temperature load was applied separately in order to ensure that the result reflected the desired preload.

In the buckle analysis, the second step is a linear perturbation buckle analysis. The first five eigenmodes are calculated. These eigenmodes are then automatically written to the input file for the general static analysis.

For the second analysis the first step is the same as for the first analysis. For the second step, the eigenmodes calculated previously are scaled down by a factor $10^{-}2$ and inserted as initial imperfections in the model. This was done in order to ensure that any buckling behaviour would be captured in the general static analysis. Further, ABAQUS was set to using non-linear geometry, in combination with plastic material properties in the beams. This step outputs stress, displacement, sectional forces in the beams and diagonals as well a plastic strain.

The output data was analyzed via the ABAQUS GUI, but also via a separate ODB (output database) python script. For an analysis of an initial reference cross section, this script makes n cuts (defined by the user) along each beam in rows A, B and C, and extracts the sectional forces and moments (resultants and components) at that cut. These are then written to a separate MATLAB-file and plotted against the entire length of the structure. The sectional resultant forces and moments are extracted. It is however also possible to analyze individual force and moment components with respect to a local coordinate system defined in the same manner for each beam. In this chapter, the resultants are presented.

Additional separate studies concerning global parameters such as boundary conditions (connection at the nave), root and tip separation, blade inclination and section length were conducted and analyzed by use of the ODB-script.

5.2 Parametric study of global parameters

Variations to the overall design of the structure were parameterized and their impact were studied, namely a change to the root and tip separations (an increase in the gross global cross section) and a hinged connection at the nave. All initial global parametric studies were conducted for a reference square cross section with a large thickness. The purpose of these studies was not necessarily to arrive at a solution to problems, but rather to study the impact such parameters had on the force and moment distributions throughout the structure.

Tampering with the sectional length in this model essentially only decreases the overall length of the structure, while keeping the number of sections constant. This is due to the number of sections not being a variable parameter. The viability of this strategy is therefore questionable as it would probably be more advantageous to instead decrease the number of sections for a decreasing overall length. Predictably, decreasing the section length decreases forces and moments in a linear fashion, as shown in figure 5.1.

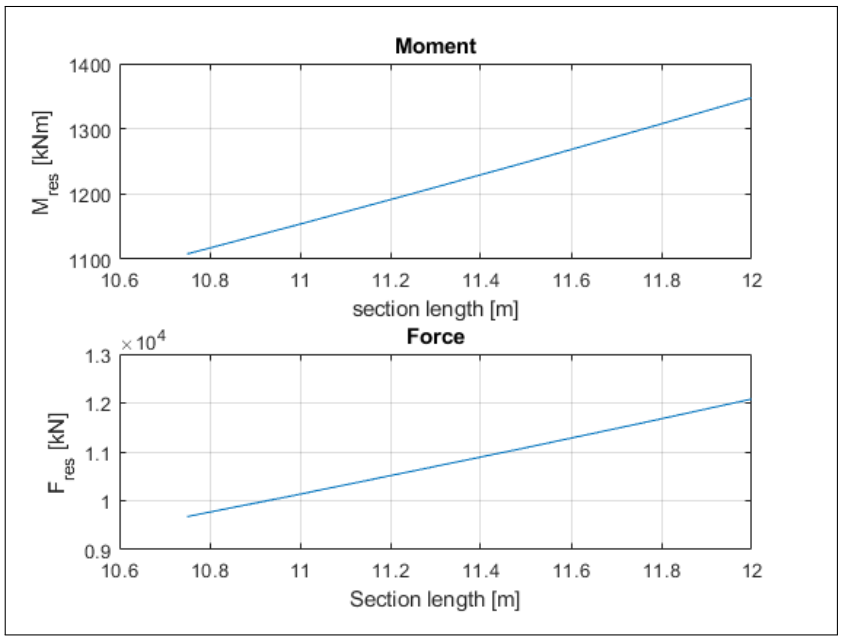

Figure 5.1: Maximum force and moments in beam row A depending on the sections length.

Increasing the root and tip separations predictably has a large impact on the stresses in the beams, as this increases the lever-arm required to counter the moment at the nave. This alteration comes at a slight increase in weight due to the increased length of diagonals and verticals. Without taking factors such as aerodynamics, production and transportation into account, this may be a cheap way to increase the stability of the structure.

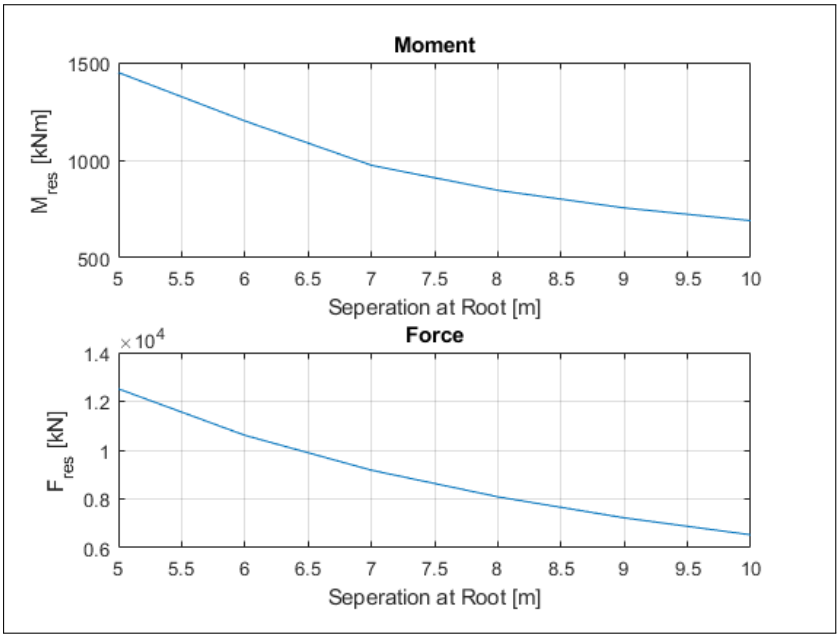

Figure 5.2: Maximum force and moments in beam row A depending on the Separation length.

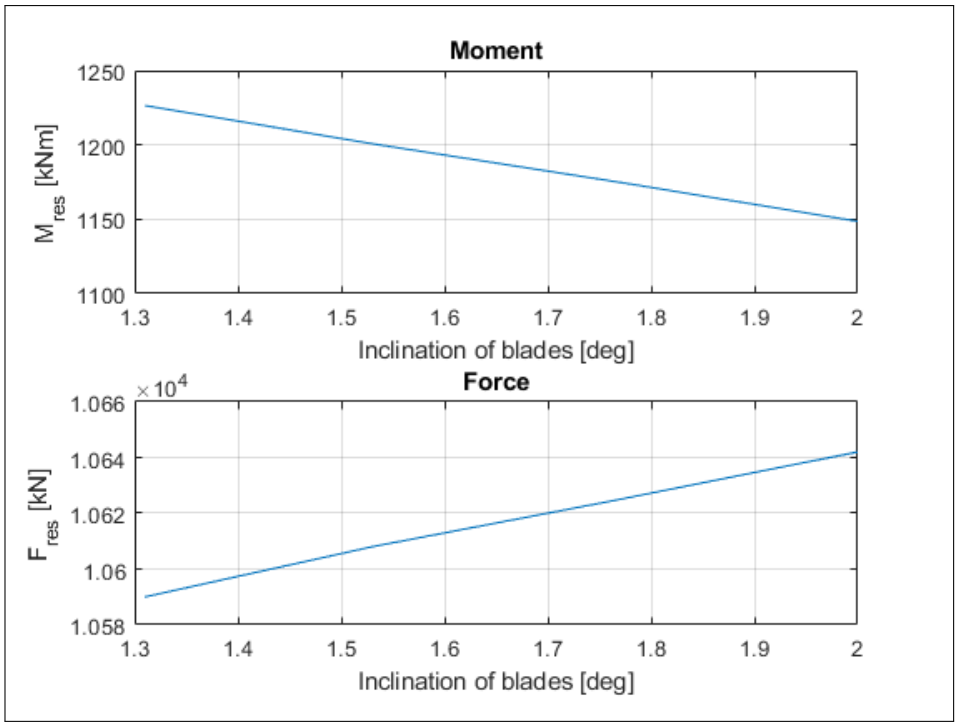

Figure 5.3: Maximum force and moments in beam row A depending on blade inclination.

Figure 5.3 shows that moments and forces decrease roughly linearly with an increasing separation at the root and tip.

The blade inclination does have a noticeable effect for small changes to the angle. This will however result in changes to the aerodynamic performance of the structure, and is therefor not deemed as a viable alteration. Increasing angles will produce a wind force resultant increasingly unfavorable for energy production.

Changing the method of connection at the nave produces (at a glance) vastly different moment diagrams, shown in figures 5.4 and 5.5.

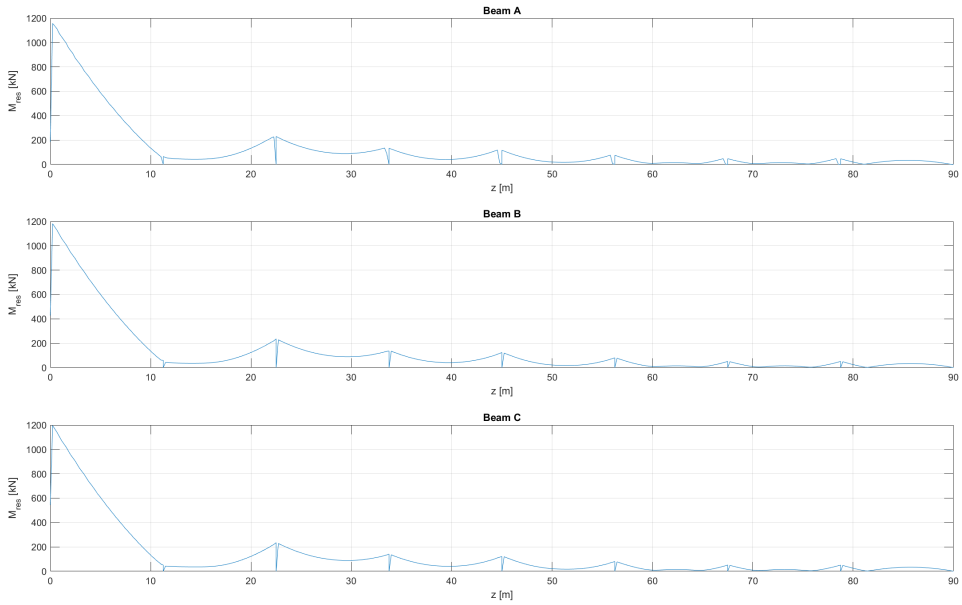

Figure 5.4: Resultant moments in beams A, B and C for a pinned nave-connection.

When studying the diagrams closer however, it may be seen that it is only the moment at the nave that changes significantly. Similarly, it can be seen that the force resultants in the beams do not change significantly, as shown in figures 5.6 and 5.7.

Still, this was deemed as the most interesting parameter to study in greater detail for a corrugated section, as the impact it would have on factors such as stress and plasticity were not easily predicted. This is discussed further in chapter 5.3.

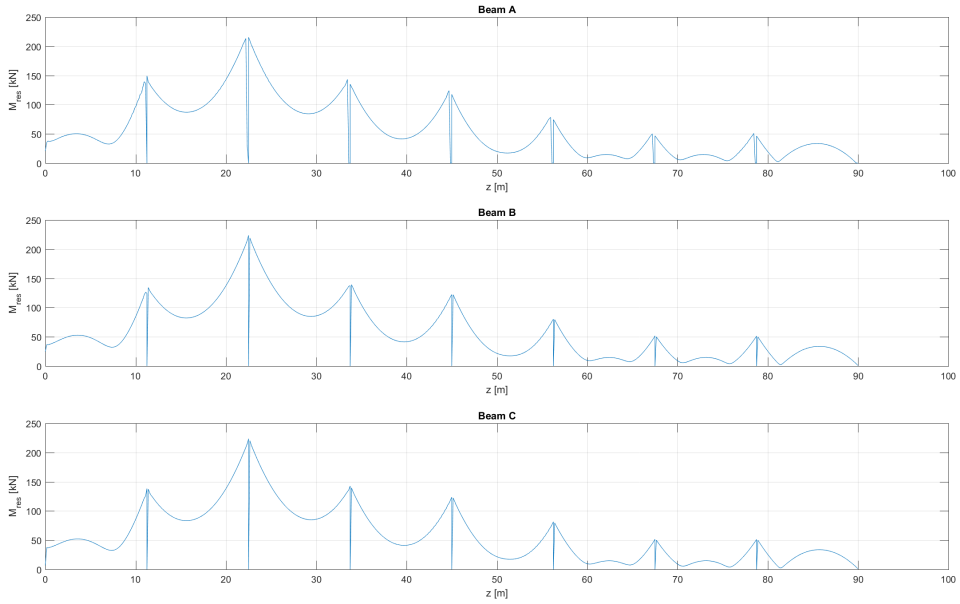

Figure 5.5: Resultant moments in beams A, B and C for a hinged nave-connection. The Moment at the nave is not zero due to the torque created about the length of the beams.

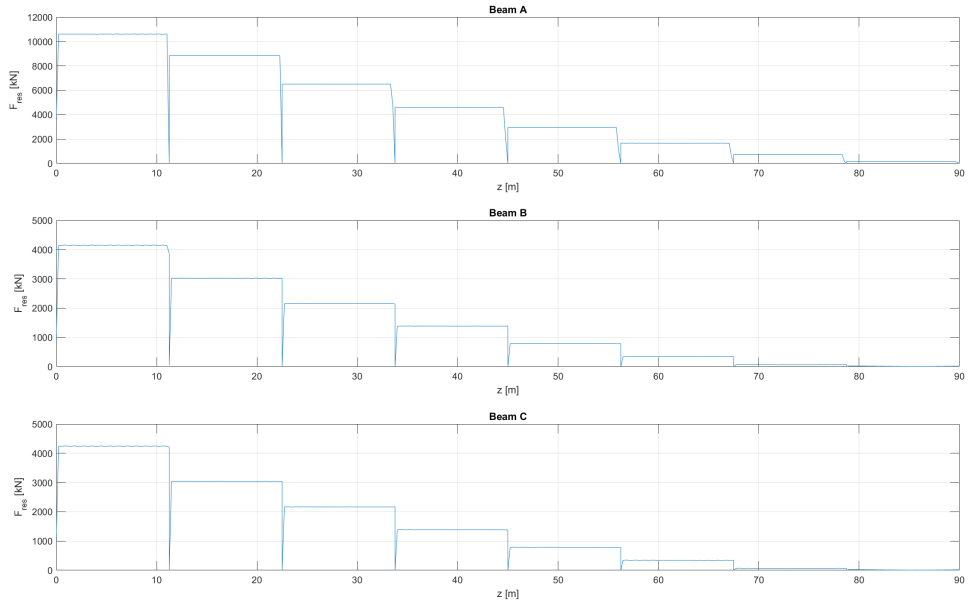

Figure 5.6: Force resultants in the beams for a pinned nave-connection.

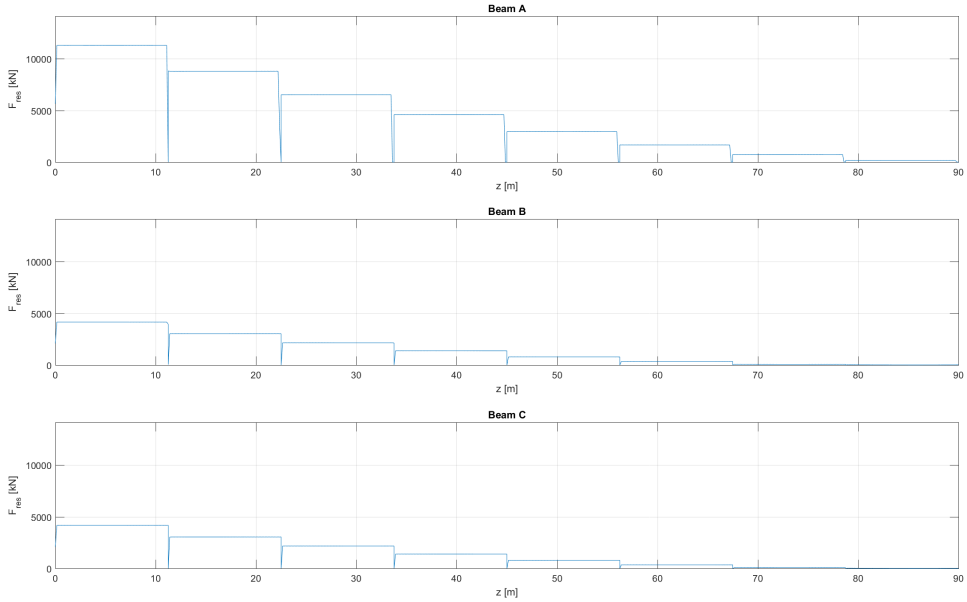

Figure 5.7: Force resultants in the beams for a hinged nave-connection.

5.3 Study of Cross sections

The cross sections were studied in two phases. The first phase being a process of elimination, where a non-linear analysis was conducted for all cross sections and a number of thicknesses. Here, the time step at which the simulations were aborted/completed was used as the deciding factor. The second phase was a study of the non-linear behaviour of the cross sections deemed to have passed the elimination process, where more detailed study of plastic behaviour and stress was studied, along with the implementation of a hinged connection at the nave.

The various cross sections analyzed are displayed in figure 5.8.

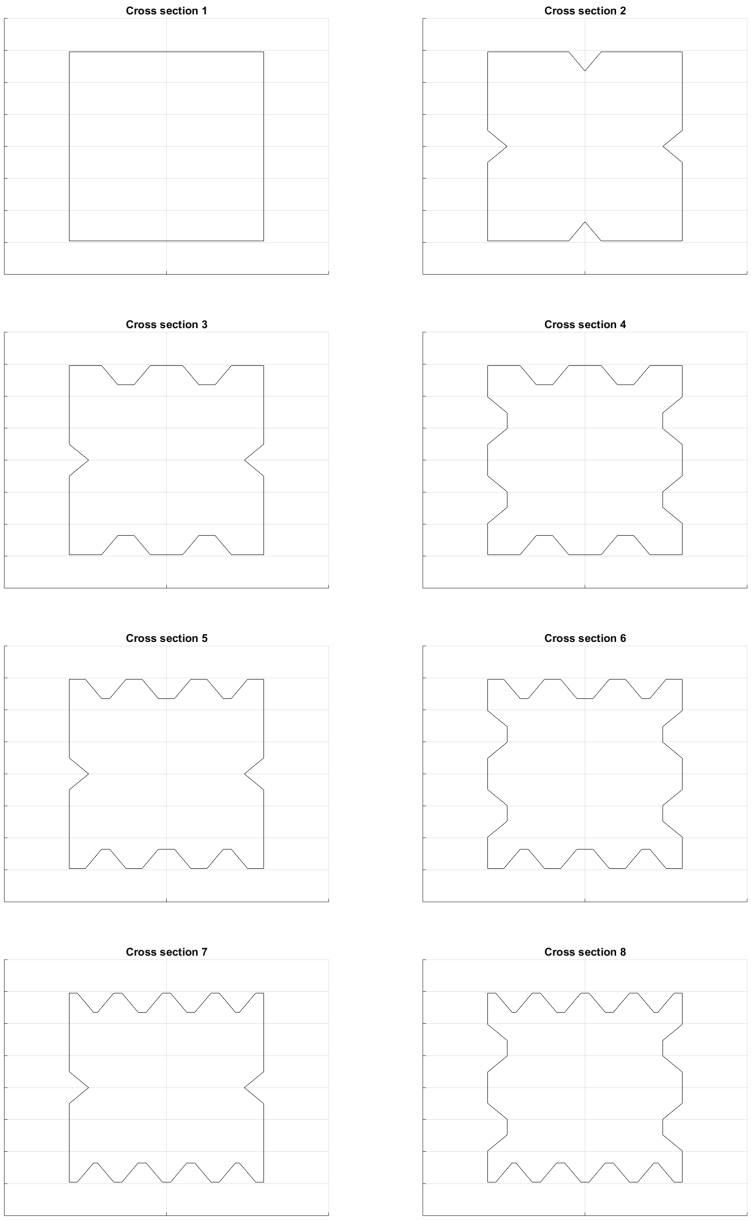

Figure 5.8: Illustration of the different cross section configurations analyzed

Thickness	Beams	Scale factor per section (initial thickness · factor)							
		1	2	3	4	5	6	7	8
T1	A	1.00	0.80	0.80	0.60	0.60	0.40	0.40	0.40
	B/C	0.90	0.70	0.70	0.50	0.50	0.30	0.30	0.30
T2	A	0.95	0.75	0.75	0.55	0.55	0.35	0.35	0.35
	B/C	0.85	0.65	0.65	0.45	0.45	0.25	0.25	0.25
T3	A	0.90	0.70	0.70	0.50	0.50	0.30	0.30	0.30
	B/C	0.80	0.60	0.60	0.40	0.40	0.20	0.20	0.20
T4	A	0.85	0.65	0.65	0.45	0.45	0.25	0.25	0.25
	B/C	0.75	0.55	0.55	0.35	0.35	0.20	0.20	0.20
T5	A	0.70	0.60	0.60	0.40	0.40	0.20	0.20	0.20
	B/C	0.60	0.50	0.50	0.30	0.30	0.20	0.20	0.20
T6	A	0.65	0.55	0.55	0.35	0.35	0.20	0.20	0.20
	B/C	0.55	0.45	0.45	0.30	0.30	0.20	0.20	0.20
T7	A	0.7	0.50	0.50	0.30	0.30	0.20	0.20	0.20
	B/C	0.55	0.50	0.50	0.30	0.30	0.20	0.20	0.20
T8	A	0.70	0.50	0.40	0.25	0.25	0.20	0.20	0.20
	B/C	0.55	0.50	0.40	0.25	0.25	0.20	0.20	0.20
T9	A	0.55	0.55	0.35	0.25	0.25	0.20	0.20	0.20
	B/C	0.55	0.40	0.35	0.25	0.25	0.20	0.20	0.20
T10	A	0.70	0.55	0.35	0.25	0.25	0.20	0.20	0.20
	B/C	0.55	0.35	0.35	0.25	0.25	0.20	0.20	0.20

Table 5.1: Scaling of the initial thickness that are set to a value for each cross section for constant mass for the thickness variations.

In order to determine which cross sections that were most suited for the structure, an iterative study was conducted for the eight cross sectional types using ten different thickness distributions, displayed in 5.1. The distributions have a constant weight for the different cross sections and are named from $T1$ to $T10$. This resulted in 80 simulations in total. All simulations were conducted using plastic material properties and non-linear geometry. In addition, the first four calculated buckling modes were applied as initial imperfections for each analysis in order to capture any post buckling behaviour characterized by these modes. These modes were scaled down, with a decreasing scale factor for higher modes. The scale factors for the first four modes were set to 0.01, 0.005, 0.0025 and 0.00125.

The cross sections were judged by their achieved time step, i.e. how much of the total load was able to be applied. Due to all loads being applied linearly over 1 s, the time step at which the simulation aborts or completes reflects what percentage of the total load the structure was able to resist. If a simulation is aborted at a timestep $t < 1$ s, the structure has not been able to resist the full load for that particular cross section and thickness. A failure to fully apply the load is due to the structure's stiffness $K \leq 0$, i.e. the equilibrium path reaching a limit point, see chapter 3.2.2.

5.3.1 Results - Bearing capacity of cross sections

Initial tests showed that it was more beneficial to use a smaller width for the cross sections. The width of the first beams A1, B1 and C1 were set to 0.6 m, as opposed to the given 0.8 m, and the following beams were scaled accordingly. The dimensions of the beams are displayed in table 5.2 below.

Section 1	Section 2	Section 3	Section 4	Section 5	Section 6	Section 7	Section 8
600x591	600x591	600x519	600x591	566x558	494x487	418x412	358x353

Table 5.2: Outer dimensions of the beams [WxH] for each section in mm.

The reason for it being more advantageous to use a smaller width is because it allows for a greater overall thickness of the cross section while still maintaining the same weight, thereby reducing the stresses in the spar and shear caps.

The results for these analyses are presented in table 5.3.

CS-type	T1	T2	T3	T4	T5	T6	T7	T8	T9	T10
1	0.63	0.48	0.38	0.32	0.15	0.17	0.11	0.07	0.07	0.09
2	**1.00**	**1.00**	**1.00**	**1.00**	0.93	0.87	0.85	0.65	0.65	0.69
3	**1.00**	**1.00**	**1.00**	**1.00**	0.97	0.91	0.96	0.88	0.79	0.87
4	**1.00**	**1.00**	**1.00**	**1.00**	**1.00**	0.96	**1.00**	**1.00**	0.82	**1.00**
5	**1.00**	**1.00**	**1.00**	**1.00**	0.96	0.90	0.96	0.83	0.79	0.83
6	**1.00**	**1.00**	**1.00**	**1.00**	**1.00**	0.91	**1.00**	**1.00**	0.85	**1.00**
7	**1.00**	**1.00**	**1.00**	**1.00**	0.96	0.91	0.96	0.87	0.72	0.72
8	**1.00**	**1.00**	**1.00**	**1.00**	**1.00**	0.97	**1.00**	**1.00**	0.85	**1.00**

Table 5.3: The results from the time step study. Values 1.0 indicate that the load was fully applied.

As can be seen, cross sectional types 4, 6 and 8 are the most promising. All are able to fully apply the load except for thickness types T6 and T9. Type T9 is lighter than T10, where the only differences are an increased thickness for beam A1 and a decrease in thickness for beams B2 and C2, and was regarded as the limit for all 3 cross sections. Time steps $t < 1$ s are to be regarded as a percentage of the load, i.e. for for cross section 1, thickness T6, a mere 17% of the load was applied before the stiffness $K \leq 0$. Judging by it's slightly higher load percentage of thickness T6, cross section 8 was deemed to be the most promising, and was thus studied further in more detail. As a final remark, it can be noted that the introduction of corrugations vastly improves the capacity of the beams. The thicknesses for each cross sectional type with a thickness type T10 are displayed in table 5.4. Here, thicknesses are listed per cross sectional type, section number and beam row. E.g., a beam in row A section 4 with cross sectional type 5 has a thickness of 2.1 mm. Using the thickness configuration T10 results in a total weight of roughly 33 tonnes.

Cross section	Sec. 1	Sec. 2	Sec. 3	Sec. 4	Sec. 5	Sec 6	Sec. 7	Sec. 8
Cross section 1 A	7.0	5.5	3.5	2.5	2.5	2.0	2.0	2.0
Cross section 1 B/C	5.5	3.5	3.5	2.5	2.5	2.0	2.0	2.0
Cross section 2 A	6.4	5	3.2	2.3	2.3	1.8	1.8	1.8
Cross section 2 B/C	5	3.2	3.2	2.3	2.3	1.8	1.8	1.8
Cross section 3 A	6.1	4.8	3.1	2.2	2.2	1.8	1.8	1.8
Cross section 3 B/C	4.8	3.1	3.1	2.2	2.2	1.8	1.8	1.8
Cross section 4 A	**5.9**	**4.6**	**2.9**	**2.1**	**2.1**	**1.7**	**1.7**	**1.7**
Cross section 4 B/C	**4.6**	**2.9**	**2.9**	**2.1**	**2.1**	**1.7**	**1.7**	**1.7**
Cross section 5 A	5.9	4.6	2.9	2.1	2.1	1.7	1.7	1.7
Cross section 5 B/C	4.6	2.9	2.9	2.1	2.1	1.7	1.7	1.7
Cross section 6 A	**5.7**	**4.4**	**2.8**	**2.0**	**2.0**	**1.6**	**1.6**	**1.6**
Cross section 6 B/C	**4.4**	**2.8**	**2.8**	**2.0**	**2.0**	**1.6**	**1.6**	**1.6**
Cross section 7 A	5.7	4.4	2.8	2.0	2.0	1.6	1.6	1.6
Cross section 7 B/C	4.4	2.8	2.8	2.0	2.0	1.6	1.6	1.6
Cross section 8 A	**5.5**	**4.3**	**2.7**	**1.9**	**1.9**	**1.6**	**1.6**	**1.6**
Cross section 8 B/C	**4.3**	**2.7**	**2.7**	**1.9**	**1.9**	**1.6**	**1.6**	**1.6**

Table 5.4: Table of the thicknesses, in mm, of the different cross section types for each sections(Sec.) with the width 0.6 m for the best of the tested thickness variation T10.

5.3.2 Study of plastic behaviour, stress and deformation.

Following the time step study, cross section 8 with thickness T10 was deemed the most suitable. This section was therefor chosen to be further analyzed concerning plasticity, stress and deformation.

First, the stresses and plastic deformations in the beams were studied in order to determine were these are the most concetrated.

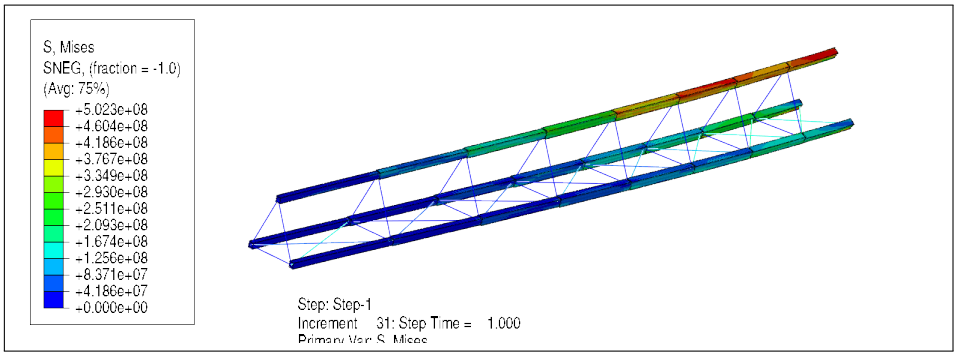

Figure 5.9: Stresses in the beams for cross sectional type 8.

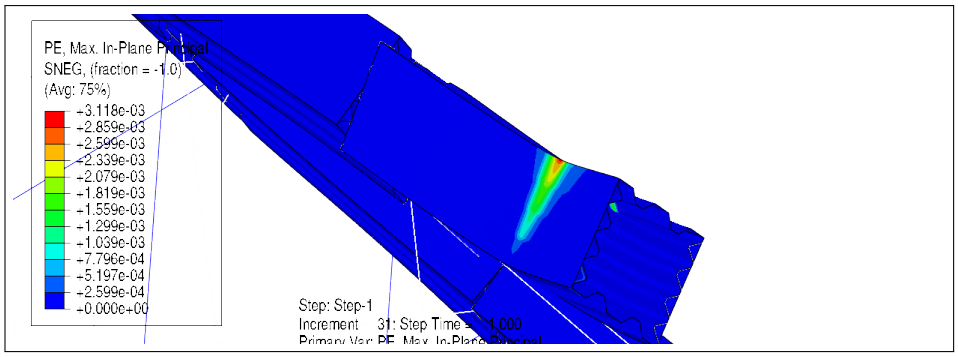

Figure 5.10: Plastic deformations. The scale has been increased to show the nature of the deformation.

The stress distribution in the beams is displayed in figure 5.9. Here, the diagonals subjected to large tensile forces have been omitted from the results. This implies that the maximum stresses rendered in the color plot will be in the beams. The distribution shows that peak stress occurs at the innermost beam A1. Here, there is indeed plastic deformation. Beam A1 exhibits a local buckling behaviour, which does not resemble the calculated modes.

The first 2 buckling modes are displayed in figures 5.11 and 5.12

As can be seen in figures 5.11 and 5.12, the first two buckling modes are global. The following three are characterized by local buckling in the outer beams, and are therefor not shown. The degree to which the calculated modes were implemented was varied, i.e. the scaling with which the modes were applied as initial imperfections was increased. This still resulted in failure to trigger these buckling modes, and local buckling was still restricted to beam A1.

The failure to trigger these buckling modes is most likely due to the structure deforming during loading, and thereby producing new buckling modes. For future work, it may be advantageous to divide the analysis into multiple steps, were e.g. half the load is applied, buckling modes are calculated, and then full load is applied. This may enable a more thorough capture of post-buckling-behaviour. Based on these results, it may be necessary to either increase the thickness of beam A1, or to introduce local reinforcements in the beam.

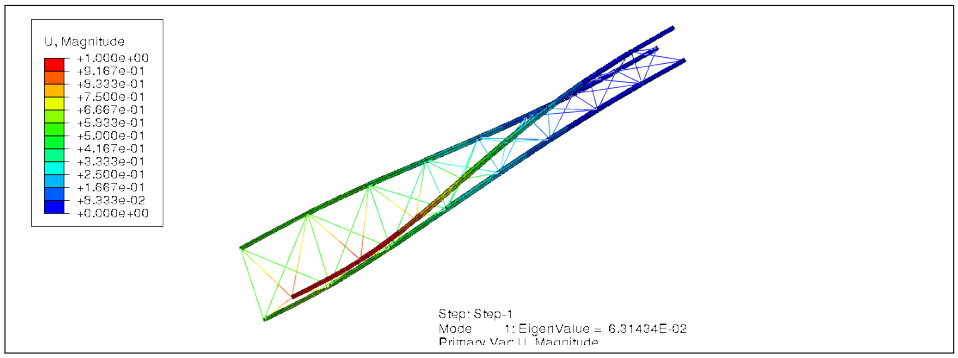

Figure 5.11: First buckling mode for cross section type 8

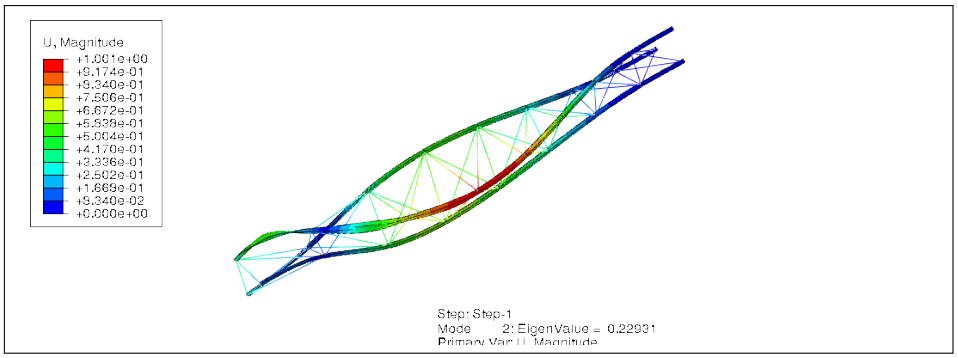

Figure 5.12: Second buckling mode for cross section type 8.

The stresses in the diagonals were also studied. The diagonals were modelled as purely elastic members, since they were assumed to be easily adaptable to higher stress ranges without significantly impacting aerodynamic performance or weight while still maintaining a sufficient stiffness.

The stresses in the diagonals are displayed in figure 5.13. Here, all members except the diagonals subjected to significant tensile forces have been omitted in order to more easily show the distribution the diagonals. As can be seen, the distribution is highest in the diagonals spanning between beams A and C, and increases in diagonals closer to the nave. The reason for the uneven distribution among the pairs is due to the torsion created by the wind. The peak stress of approx. 567 MPa is not alarmingly high, and should be able to be accounted for.

In order to determine the impact of plastic deformations on the global structure, an elastic analysis was also conducted. This enabled the comparison of elastic and plastic deformations.

As can be seen by comparing figures 5.14 and 5.15, the impact of the plastic behaviour is rather small. As can be expected, the deformation magnitude is largest at the tip. The elastic analysis yielded a maximum deflection of 2.64 m at the tip, and the plastic analysis yielded 2.67 m. I.e., the total plastic deformation is 0.03 m, or 0.33 ‰with respect to the total length of the structure. This is not regarded as a failure.

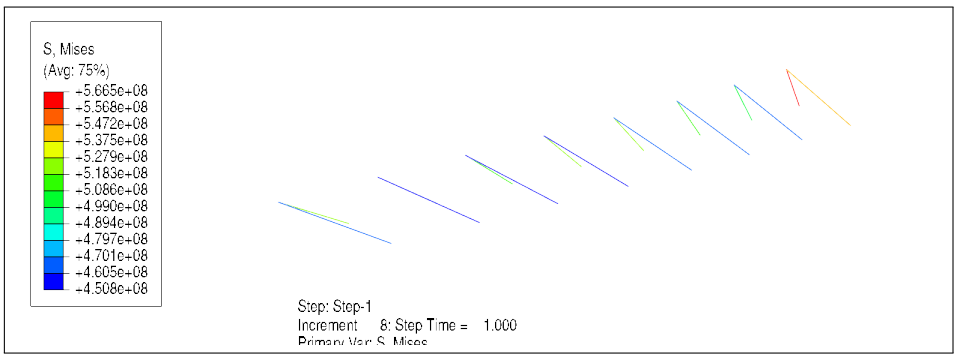

Figure 5.13: Stresses in diagonals subjected to the most significant tensile forces.

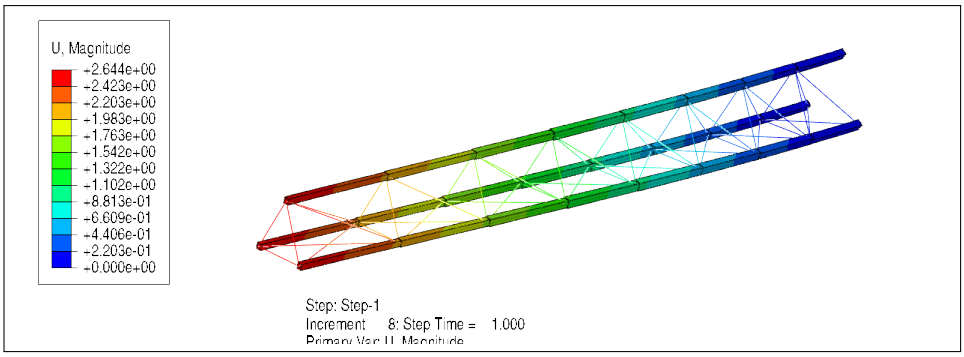

Figure 5.14: Deformation of the structure during a purely elastic analysis.

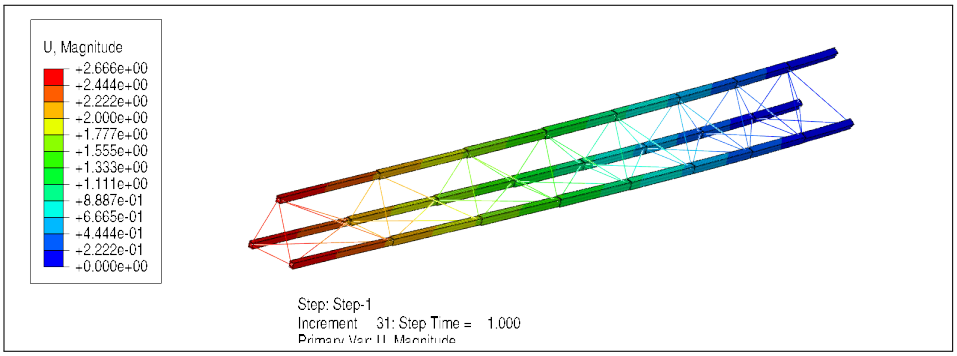

Figure 5.15: Deformation of the structure with plastic material properties enabled.

5.3.3 Impact of hinged connection

The impact of a hinged connection was also studied. This was done since initial results showed a greatly reduced moments in the first beams A1, B1 and C1. The stress distributions in the beams and diagonals were once again studied using plastic material properties.

While it may not be obvious from the stress distribution shown in figure 5.16, the peak stress region has now moved from beam A1 and is situated in between beams A2 and A3. This is to be expected, since the global analysis of the initial cross section generated a moment distribution as shown in figure 5.5. This does indeed result in plastic deformations in this region, as shown in figure 5.17.

Stresses in the diagonals were again studied, and the stress distribution is shown in figure 5.18 below.

As can be expected, a hinged connection results in larger tensile forces in the diagonals, in particular in the pair closest to the nave. Here the peak stress has increased from 567 MPa to 713 MPa. Considering that a hinged connection does not seem to eliminate plasticity in the beams, instead only redistributing it, the hinged connection does not seem to offer any significant advantages over the conventional pinned connection.

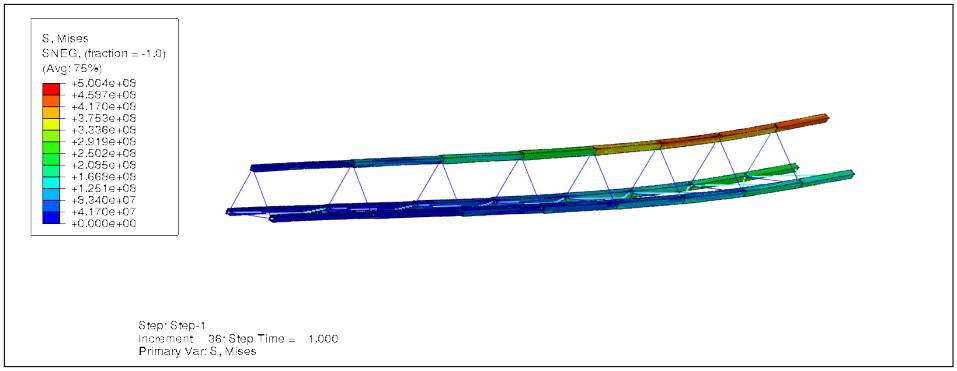

Figure 5.16: Stresses in the beams for a hinged connection at the nave, cross section 8.

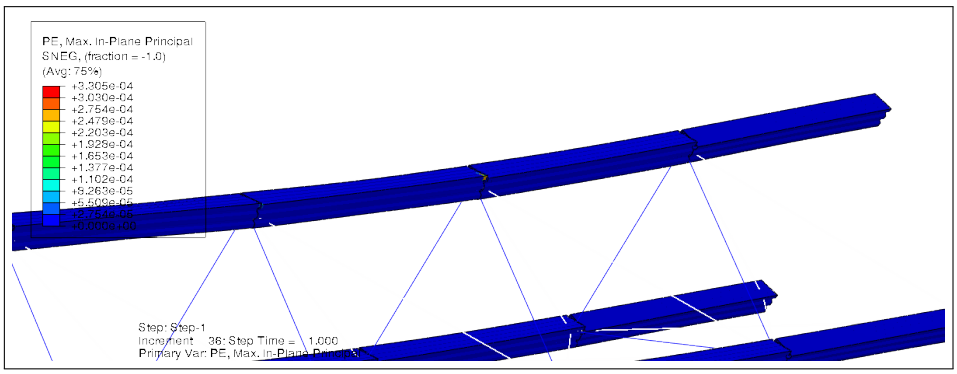

Figure 5.17: Plastic deformations occur at the interface between beam A2 and A3, where the moment is at it's highest.

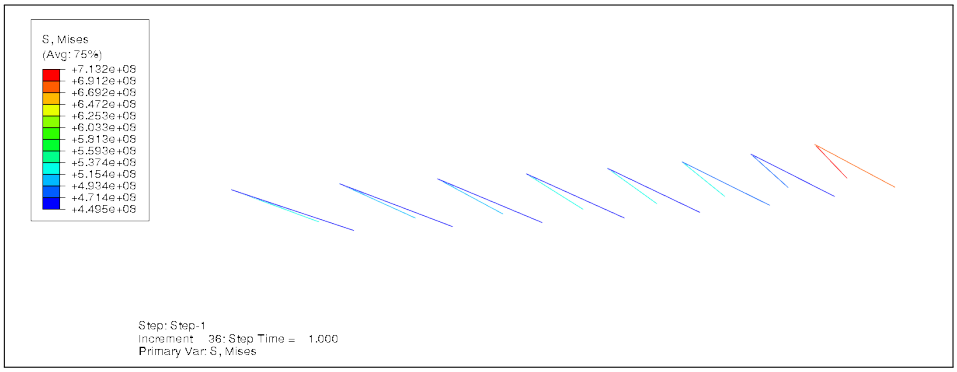

Figure 5.18: Stress distribution in the diagonals for a hinged connection.

6 Discussion

6.1 Model

As evident from the results, the first five buckling modes are not triggered during the static analysis, in spite of these having been applied as scaled down initial imperfections. This is most probably due to the fact that the buckling modes are calculated for the structure's undeformed state. When loading is applied, it is possible that deformations sufficiently large to alter the buckling modes occur.

It is unknown how plastic properties in the diagonals would impact the simulations, since these properties were omitted. This was justified by reasoning that it should be fairly simple to adjust the diagonals, either by material or cross sectional area, in such a way that they do not exceed their load bearing capacity. Having purely elastic behaviour in the diagonals was advantageous when conducting the various parametric studies, as it made it easier to distinguish between the effects of other variables, such as cross sectional types.

The influence of the airfoils themselves has been largely neglected. It is reasonable to assume that the airfoil will have a significant impact on both the global and local stability of the structure, as the airfoil drastically increases the gross width of the beam-foil assembly, see figure 2.5. The increase in width should have a large impact on the out-of-plane-buckling of the structure. For example, the first global buckling mode, displayed in figure 6.1, shows the A-beams bending out of plane in a direction which should be significantly stiffened by the airfoils.

It was difficult do discern the impact of the plates along the spar caps. The plates were a necessary addition to the model in order to reliably apply the loads, and as a result no simulations were conducted with the absence of plates. They are however in practice a viable option when considering the final design. When calculating the linear buckling modes, no cross sections displayed tendencies towards local buckling of the spar caps, which may well

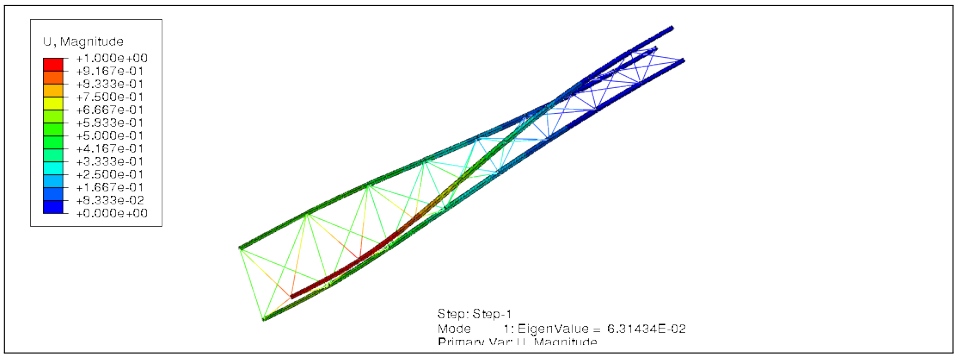

Figure 6.1: First buckling mode for cross section type 8 with a width of 600mm.

be a result of the additional stability provided by the plates.

The plastic properties used to model the steel in the beams were somewhat simplified, as the effects of plastic hardening are largely omitted. This places the simulations on the conservative side. The actual elasto-plastic properties used in the final design were unknown at the time when the studies were conducted, and as such it was deemed sufficient to assume a more idealized material behaviour, since this should still suffice to give good indications on the impact of various design alterations in the model.

The connections at the intersect of diagonals, verticals and beams are idealized to a truss system. This corresponds to the line of action of the different members intersecting at the point of connection. While this arrangement is desirable, it may in practice be somewhat difficult to achieve due to the small inclination of the diagonals. That is, an assembly where all forces act through the same point. The final design may very well have an assembly where the forces will act offset from the beam joints, and thereby causing moments.

In the final design, these forces may induce extra bending moments in the beams, thereby further decreasing stability.

7 Conclusion

From the simulations and set criteria it was determined that, of the cross sectional types tested, types 4, 6 and 8 showed the most promising results. These types allow for a significant reduction in thickness while still maintaining good overall structural integrity. Some minor plastic deformations occur in beam A1 for all types. This should however be easily overcome, either by increasing the thickness slightly or by introducing local reinforcement at the affected area. The local buckling exhibited in these areas is most likely due to the higher pitch angle of beam A1.

From the analyses, it can be seen that the linearly calculated buckling modes do not have any effect on the structure during loading. This is most likely due to the large deformations that largely alters the stress distribution and geometry of the structure and therefore the non-linearly calculated buckle modes differs from the linearly calculated before loading.

The stresses in the most loaded diagonals in some cases exceeds the maximum tensile strength most common structural steels, most notably in the innermost section. Here, a high strength material or an increased cross sectional area of the diagonals will be needed.

The total weight of the structure, regardless of cross sectional type, is roughly 33 tonnes. This exceeds the initially set criteria of 25 tonnes.

The most important conclusion from all the simulations is the marked effect of corrugated beams. Introducing corrugations drastically improves stability while also allowing for a reduction in weight. While it may not be possible to achiev the target weight of 25 tonnes, which would allow for mounting of the Triblade on existing wind farms is naturally very desirable, corrugated beams have nonetheless proven to be a very attractive proposal and should be investigated further.

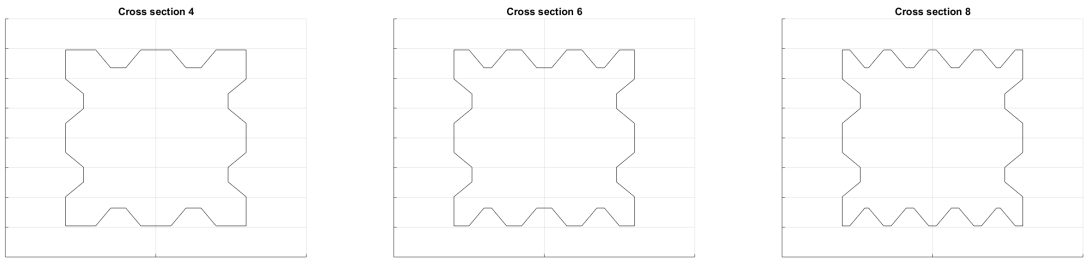

Figure 7.1: Cross section types 4, 6 and 8.

7.1 Future work

During this thesis, most of the time spent was dedicated to modeling and writing the Python-script. Other students or employees may in the future make use of the script, which is highly adaptable, and provides an easy way of testing different cross sections in a global setting.

Some suggestions for further parametric investigations include:

- Studying the impact of using different materials, including other steel types.
- Studying the independent alteration of thicknesses of spar and shear caps.
- Studying different types of connections at the intersections of beams, diagonals and verticals (methods which induce moments).
- Determining the influence of the airfoils on local and global stability.
- Conducting a full analysis containing both the stand still load case as well as the production load case to further improve the design.

Bibliography

Brøndsted, Povl, Hans Lilholt and Aage Lystrup (2005). "COMPOSITE MATERIALS FOR WIND POWER TURBINE BLADES". In: *Annual Review of Materials Research* 35.1, pp. 505–538.

Dassault Systèmes (2015). *Abaqus/CAE User's Guide*.

Det Norske Veritas, Risø National Laboratory (2002). *Guidelines for Design of Wind turbines*. Tech. rep.

McGinty, B. *Column buckling*. URL: `http://www.continuummechanics.org/columnbuckling.html` (visited on 12/03/2019).

Ottosen, Hans Petersson & Niels Saabye (1992). *Introduction to the Finite Element Method*. English. Prentice Hall.

Persson, Kent (2018). *Course: Finite Element Method, Structural Analysis (VSMN30),Lecture in Non-linear Material.*

Riks, E (1979). "An incremental approach to the solution of snapping and buckling problems". In: *International Journal of Solids and Structures*.

Ristinmaa, M (2018). *Introduction to Non-linear Finite element method*. Swedish.

Wadsö, Lars (2015). *Construction Materials Science*. Reading, Massachusetts: Building materials, Lund University.

Winfoor. *Drag Coefficient*. URL: `http://winfoor.com/company/` (visited on 22/05/2019).

Cross section type 1	Sec. 1	Sec. 2	Sec. 3	Sec. 4	Sec. 5	Sec. 6	Sec. 7	Sec. 8
T1 Beam A	10.0	8.0	8.0	6.0	6.0	4.0	4.0	4.0
T1 Beam B/C	9.0	7.0	7.0	5.0	5.0	3.0	3.0	3.0
T2 Beam A	9.5	7.5	7.5	5.5	5.5	3.5	3.5	3.5
T2 Beam B/C	8.5	6.5	6.5	4.5	4.5	2.5	2.5	2.5
T3 Beam A	9.0	7.0	7.0	5.0	5.0	3.0	3.0	3.0
T3 Beam B/C	8.0	6.0	6.0	4.0	4.0	2.0	2.0	2.0
T4 Beam A	8.5	6.5	6.5	4.5	4.5	2.5	2.5	2.5
T4 Beam B/C	7.5	5.5	5.5	3.5	3.5	2.0	2.0	2.0
T5 Beam A	7.0	6.0	6.0	4.0	4.0	2.0	2.0	2.0
T5 Beam B/C	6.0	5.0	5.0	3.0	3.0	2.0	2.0	2.0
T6 Beam A	6.5	5.5	5.5	3.5	3.5	2.0	2.0	2.0
T6 Beam B/C	5.5	4.5	4.5	3.0	3.0	2.0	2.0	2.0
T7 Beam A	7.0	5.0	5.0	3.0	3.0	2.0	2.0	2.0
T7 Beam B/C	5.5	5.0	5.0	3.0	3.0	2.0	2.0	2.0
T8 Beam A	7.0	5.0	4.0	2.5	2.5	2.0	2.0	2.0
T8 Beam B/C	5.5	5.0	4.0	2.5	2.5	2.0	2.0	2.0
T9 Beam A	5.5	5.5	3.5	2.5	2.5	2.0	2.0	2.0
T9 Beam B/C	5.5	4.0	3.5	2.5	2.5	2.0	2.0	2.0
T10 Beam A	7.0	5.5	3.5	2.5	2.5	2.0	2.0	2.0
T10 Beam B/C	5.5	3.5	3.5	2.5	2.5	2.0	2.0	2.0

Table 1: Thicknesses for the different sections in (mm) tested for Cross section 1

Cross section type 2	Sec. 1	Sec. 2	Sec. 3	Sec. 4	Sec. 5	Sec. 6	Sec. 7	Sec. 8
T1 Beam A	9.1	7.3	7.3	5.5	5.5	3.7	3.7	3.7
T1 Beam B/C	8.2	6.4	6.4	4.6	4.6	2.7	2.7	2.7
T2 Beam A	8.7	6.9	6.9	5.0	5.0	3.2	3.2	3.2
T2 Beam B/C	7.8	5.9	5.9	4.1	4.1	2.3	2.3	2.3
T3 Beam A	8.2	6.4	6.4	4.6	4.6	2.7	2.7	2.7
T3 Beam B/C	7.3	5.5	5.5	3.7	3.7	1.8	1.8	1.8
T4 Beam A	7.8	5.9	5.9	4.1	4.1	2.3	2.3	2.3
T4 Beam B/C	6.9	5.0	5.0	3.2	3.2	1.8	1.8	1.8
T5 Beam A	6.4	5.5	5.5	3.7	3.7	1.8	1.8	1.8
T5 Beam B/C	5.5	4.6	4.6	2.7	2.7	1.8	1.8	1.8
T6 Beam A	5.9	5.0	5.0	3.2	3.2	1.8	1.8	1.8
T6 Beam B/C	5.0	4.1	4.1	2.7	2.7	1.8	1.8	1.8
T7 Beam A	6.4	4.6	4.6	2.7	2.7	1.8	1.8	1.8
T7 Beam B/C	5.0	4.6	4.6	2.7	2.7	1.8	1.8	1.8
T8 Beam A	6.4	4.6	3.7	2.3	2.3	1.8	1.8	1.8
T8 Beam B/C	5.0	4.6	3.7	2.3	2.3	1.8	1.8	1.8
T9 Beam A	5.0	5.0	3.2	2.3	2.3	1.8	1.8	1.8
T9 Beam B/C	5.0	3.7	3.2	2.3	2.3	1.8	1.8	1.8
T10 Beam A	6.4	5.0	3.2	2.3	2.3	1.8	1.8	1.8
T10 Beam B/C	5.0	3.2	3.2	2.3	2.3	1.8	1.8	1.8

Table 2: Thicknesses for the different sections in (mm) tested for Cross section 2

Cross section type 3	Sec. 1	Sec. 2	Sec. 3	Sec. 4	Sec. 5	Sec. 6	Sec. 7	Sec. 8
T1 Beam A	8.8	7.0	7.0	5.3	5.3	3.5	3.5	3.5
T1 Beam B/C	7.9	6.1	6.1	4.4	4.4	2.6	2.6	2.6
T2 Beam A	8.3	6.6	6.6	4.8	4.8	3.1	3.1	3.1
T2 Beam B/C	7.4	5.7	5.7	3.9	3.9	2.2	2.2	2.2
T3 Beam A	7.9	6.1	6.1	4.4	4.4	2.6	2.6	2.6
T3 Beam B/C	7.0	5.3	5.3	3.5	3.5	1.8	1.8	1.8
T4 Beam A	7.4	5.7	5.7	3.9	3.9	2.2	2.2	2.2
T4 Beam B/C	6.6	4.8	4.8	3.1	3.1	1.8	1.8	1.8
T5 Beam A	6.1	5.3	5.3	3.5	3.5	1.8	1.8	1.8
T5 Beam B/C	5.3	4.4	4.4	2.6	2.6	1.8	1.8	1.8
T6 Beam A	5.7	4.8	4.8	3.1	3.1	1.8	1.8	1.8
T6 Beam B/C	4.8	3.9	3.9	2.6	2.6	1.8	1.8	1.8
T7 Beam A	6.1	4.4	4.4	2.6	2.6	1.8	1.8	1.8
T7 Beam B/C	4.8	4.4	4.4	2.6	2.6	1.8	1.8	1.8
T8 Beam A	6.1	4.4	3.5	2.2	2.2	1.8	1.8	1.8
T8 Beam B/C	4.8	4.4	3.5	2.2	2.2	1.8	1.8	1.8
T9 Beam A	4.8	4.8	3.1	2.2	2.2	1.8	1.8	1.8
T9 Beam B/C	4.8	3.5	3.1	2.2	2.2	1.8	1.8	1.8
T10 Beam A	6.1	4.8	3.1	2.2	2.2	1.8	1.8	1.8
T10 Beam B/C	4.8	3.1	3.1	2.2	2.2	1.8	1.8	1.8

Table 3: Thicknesses for the different sections in (mm) tested for Cross section 3

Cross section type 4	Sec. 1	Sec. 2	Sec. 3	Sec. 4	Sec. 5	Sec. 6	Sec. 7	Sec. 8
T1 Beam A	8.4	6.7	6.7	5.0	5.0	3.4	3.4	3.4
T1 Beam B/C	7.6	5.9	5.9	4.2	4.2	2.5	2.5	2.5
T2 Beam A	8.0	6.3	6.3	4.6	4.6	2.9	2.9	2.9
T2 Beam B/C	7.2	5.5	5.5	3.8	3.8	2.1	2.1	2.1
T3 Beam A	7.6	5.9	5.9	4.2	4.2	2.5	2.5	2.5
T3 Beam B/C	6.7	5.0	5.0	3.4	3.4	1.7	1.7	1.7
T4 Beam A	7.2	5.5	5.5	3.8	3.8	2.1	2.1	2.1
T4 Beam B/C	6.3	4.6	4.6	2.9	2.9	1.7	1.7	1.7
T5 Beam A	5.9	5.0	5.0	3.4	3.4	1.7	1.7	1.7
T5 Beam B/C	5.0	4.2	4.2	2.5	2.5	1.7	1.7	1.7
T6 Beam A	5.5	4.6	4.6	2.9	2.9	1.7	1.7	1.7
T6 Beam B/C	4.6	3.8	3.8	2.5	2.5	1.7	1.7	1.7
T7 Beam A	5.9	4.2	4.2	2.5	2.5	1.7	1.7	1.7
T7 Beam B/C	4.6	4.2	4.2	2.5	2.5	1.7	1.7	1.7
T8 Beam A	5.9	4.2	3.4	2.1	2.1	1.7	1.7	1.7
T8 Beam B/C	4.6	4.2	3.4	2.1	2.1	1.7	1.7	1.7
T9 Beam A	4.6	4.6	2.9	2.1	2.1	1.7	1.7	1.7
T9 Beam B/C	4.6	3.4	2.9	2.1	2.1	1.7	1.7	1.7
T10 Beam A	5.9	4.6	2.9	2.1	2.1	1.7	1.7	1.7
T10 Beam B/C	4.6	2.9	2.9	2.1	2.1	1.7	1.7	1.7

Table 4: Thicknesses for the different sections in (mm) tested for Cross section 4

Cross section type 5	Sec. 1	Sec. 2	Sec. 3	Sec. 4	Sec. 5	Sec. 6	Sec. 7	Sec. 8
T1 Beam A	8.4	6.7	6.7	5.0	5.0	3.4	3.4	3.4
T1 Beam B/C	7.6	5.9	5.9	4.2	4.2	2.5	2.5	2.5
T2 Beam A	8.0	6.3	6.3	4.6	4.6	2.9	2.9	2.9
T2 Beam B/C	7.2	5.5	5.5	3.8	3.8	2.1	2.1	2.1
T3 Beam A	7.6	5.9	5.9	4.2	4.2	2.5	2.5	2.5
T3 Beam B/C	6.7	5.0	5.0	3.4	3.4	1.7	1.7	1.7
T4 Beam A	7.2	5.5	5.5	3.8	3.8	2.1	2.1	2.1
T4 Beam B/C	6.3	4.6	4.6	2.9	2.9	1.7	1.7	1.7
T5 Beam A	5.9	5.0	5.0	3.4	3.4	1.7	1.7	1.7
T5 Beam B/C	5.0	4.2	4.2	2.5	2.5	1.7	1.7	1.7
T6 Beam A	5.5	4.6	4.6	2.9	2.9	1.7	1.7	1.7
T6 Beam B/C	4.6	3.8	3.8	2.5	2.5	1.7	1.7	1.7
T7 Beam A	5.9	4.2	4.2	2.5	2.5	1.7	1.7	1.7
T7 Beam B/C	4.6	4.2	4.2	2.5	2.5	1.7	1.7	1.7
T8 Beam A	5.9	4.2	3.4	2.1	2.1	1.7	1.7	1.7
T8 Beam B/C	4.6	4.2	3.4	2.1	2.1	1.7	1.7	1.7
T9 Beam A	4.6	4.6	2.9	2.1	2.1	1.7	1.7	1.7
T9 Beam B/C	4.6	3.4	2.9	2.1	2.1	1.7	1.7	1.7
T10 Beam A	5.9	4.6	2.9	2.1	2.1	1.7	1.7	1.7
T10 Beam B/C	4.6	2.9	2.9	2.1	2.1	1.7	1.7	1.7

Table 5: Thicknesses for the different sections in (mm) tested for Cross section 6

Cross section type 6	Sec. 1	Sec. 2	Sec. 3	Sec. 4	Sec. 5	Sec. 6	Sec. 7	Sec. 8
T1 Beam A	8.1	6.5	6.5	4.9	4.9	3.2	3.2	3.2
T1 Beam B/C	7.3	5.7	5.7	4.0	4.0	2.4	2.4	2.4
T2 Beam A	7.7	6.1	6.1	4.4	4.4	2.8	2.8	2.8
T2 Beam B/C	6.9	5.3	5.3	3.6	3.6	2.0	2.0	2.0
T3 Beam A	7.3	5.7	5.7	4.0	4.0	2.4	2.4	2.4
T3 Beam B/C	6.5	4.9	4.9	3.2	3.2	1.6	1.6	1.6
T4 Beam A	6.9	5.3	5.3	3.6	3.6	2.0	2.0	2.0
T4 Beam B/C	6.1	4.4	4.4	2.8	2.8	1.6	1.6	1.6
T5 Beam A	5.7	4.9	4.9	3.2	3.2	1.6	1.6	1.6
T5 Beam B/C	4.9	4.0	4.0	2.4	2.4	1.6	1.6	1.6
T6 Beam A	5.3	4.4	4.4	2.8	2.8	1.6	1.6	1.6
T6 Beam B/C	4.4	3.6	3.6	2.4	2.4	1.6	1.6	1.6
T7 Beam A	5.7	4.0	4.0	2.4	2.4	1.6	1.6	1.6
T7 Beam B/C	4.4	4.0	4.0	2.4	2.4	1.6	1.6	1.6
T8 Beam A	5.7	4.0	3.2	2.0	2.0	1.6	1.6	1.6
T8 Beam B/C	4.4	4.0	3.2	2.0	2.0	1.6	1.6	1.6
T9 Beam A	4.4	4.4	2.8	2.0	2.0	1.6	1.6	1.6
T9 Beam B/C	4.4	3.2	2.8	2.0	2.0	1.6	1.6	1.6
T10 Beam A	5.7	4.4	2.8	2.0	2.0	1.6	1.6	1.6
T10 Beam B/C	4.4	2.8	2.8	2.0	2.0	1.6	1.6	1.6

Table 6: Thicknesses for the different sections in (mm) tested for Cross section 6

Cross section type 7	Sec. 1	Sec. 2	Sec. 3	Sec. 4	Sec. 5	Sec. 6	Sec. 7	Sec. 8
T1 Beam A	8.1	6.5	6.5	4.9	4.9	3.2	3.2	3.2
T1 Beam B/C	7.3	5.7	5.7	4.0	4.0	2.4	2.4	2.4
T2 Beam A	7.7	6.1	6.1	4.4	4.4	2.8	2.8	2.8
T2 Beam B/C	6.9	5.3	5.3	3.6	3.6	2.0	2.0	2.0
T3 Beam A	7.3	5.7	5.7	4.0	4.0	2.4	2.4	2.4
T3 Beam B/C	6.5	4.9	4.9	3.2	3.2	1.6	1.6	1.6
T4 Beam A	6.9	5.3	5.3	3.6	3.6	2.0	2.0	2.0
T4 Beam B/C	6.1	4.4	4.4	2.8	2.8	1.6	1.6	1.6
T5 Beam A	5.7	4.9	4.9	3.2	3.2	1.6	1.6	1.6
T5 Beam B/C	4.9	4.0	4.0	2.4	2.4	1.6	1.6	1.6
T6 Beam A	5.3	4.4	4.4	2.8	2.8	1.6	1.6	1.6
T6 Beam B/C	4.4	3.6	3.6	2.4	2.4	1.6	1.6	1.6
T7 Beam A	5.7	4.0	4.0	2.4	2.4	1.6	1.6	1.6
T7 Beam B/C	4.4	4.0	4.0	2.4	2.4	1.6	1.6	1.6
T8 Beam A	5.7	4.0	3.2	2.0	2.0	1.6	1.6	1.6
T8 Beam B/C	4.4	4.0	3.2	2.0	2.0	1.6	1.6	1.6
T9 Beam A	4.4	4.4	2.8	2.0	2.0	1.6	1.6	1.6
T9 Beam B/C	4.4	3.2	2.8	2.0	2.0	1.6	1.6	1.6
T10 Beam A	5.7	4.4	2.8	2.0	2.0	1.6	1.6	1.6
T10 Beam B/C	4.4	2.8	2.8	2.0	2.0	1.6	1.6	1.6

Table 7: Thicknesses for the different sections in (mm) tested for Cross section 7

Cross section type 7	Sec. 1	Sec. 2	Sec. 3	Sec. 4	Sec. 5	Sec. 6	Sec. 7	Sec. 8
T1 Beam A	7.8	6.2	6.2	4.7	4.7	3.1	3.1	3.1
T1 Beam B/C	7.0	5.5	5.5	3.9	3.9	2.3	2.3	2.3
T2 Beam A	7.4	5.8	5.8	4.3	4.3	2.7	2.7	2.7
T2 Beam B/C	6.6	5.1	5.1	3.5	3.5	1.9	1.9	1.9
T3 Beam A	7.0	5.5	5.5	3.9	3.9	2.3	2.3	2.3
T3 Beam B/C	6.2	4.7	4.7	3.1	3.1	1.6	1.6	1.6
T4 Beam A	6.6	5.1	5.1	3.5	3.5	1.9	1.9	1.9
T4 Beam B/C	5.8	4.3	4.3	2.7	2.7	1.6	1.6	1.6
T5 Beam A	5.5	4.7	4.7	3.1	3.1	1.6	1.6	1.6
T5 Beam B/C	4.7	3.9	3.9	2.3	2.3	1.6	1.6	1.6
T6 Beam A	5.1	4.3	4.3	2.7	2.7	1.6	1.6	1.6
T6 Beam B/C	4.3	3.5	3.5	2.3	2.3	1.6	1.6	1.6
T7 Beam A	5.5	3.9	3.9	2.3	2.3	1.6	1.6	1.6
T7 Beam B/C	4.3	3.9	3.9	2.3	2.3	1.6	1.6	1.6
T8 Beam A	5.5	3.9	3.1	1.9	1.9	1.6	1.6	1.6
T8 Beam B/C	4.3	3.9	3.1	1.9	1.9	1.6	1.6	1.6
T9 Beam A	4.3	4.3	2.7	1.9	1.9	1.6	1.6	1.6
T9 Beam B/C	4.3	3.1	2.7	1.9	1.9	1.6	1.6	1.6
T10 Beam A	5.5	4.3	2.7	1.9	1.9	1.6	1.6	1.6
T10 Beam B/C	4.3	2.7	2.7	1.9	1.9	1.6	1.6	1.6

Table 8: Thicknesses for the different sections in (mm) tested for Cross section 8